Photoelectron spectroscopy of $HCCN^-$ and $HCNC^-$ reveals the quasilinear triplet carbenes, HCCN and HCNC

Mark R. Nimlos[a)]
National Renewable Energy Laboratory, Golden, Colorado 80401 and
Department of Chemistry and Biochemistry, University of Colorado, Boulder, Colorado 80309-0215

Gustavo Davico[b)]
JILA, University of Colorado, Boulder, Colorado 80309-0440

C. Michael Geise
Department of Chemistry, Ohio State University, Columbus, Ohio 43210-1173

Paul G. Wenthold[c)]
JILA, University of Colorado, Boulder, Colorado 80309-0440

W. Carl Lineberger[d)]
Department of Chemistry and Biochemistry, University of Colorado, Boulder, Colorado 80309-0215 and
JILA, University of Colorado, Boulder, Colorado 80309-0440

Stephen J. Blanksby
Department of Chemistry and Biochemistry, University of Colorado, Boulder, Colorado 80309-0215

Christopher M. Hadad[e)]
Department of Chemistry, Ohio State University, Columbus, Ohio 43210-1173

George A. Petersson[f)]
Hall-Atwater Laboratories, Department of Chemistry, Weleyan University, Middletown, Connecticut 06459

G. Barney Ellison[g)]
Department of Chemistry and Biochemistry, University of Colorado, Boulder, Colorado 80309-0215

(Received 5 April 2002; accepted 4 June 2002)

Negative ion photoelectron spectroscopy has been used to study the $HCCN^-$ and $HCNC^-$ ions. The electron affinities (EA) of cyanocarbene have been measured to be EA(HCCN $\tilde{X}\,^3\Sigma^- = 2.003 \pm 0.014$ eV and EA(DCCN $\tilde{X}\,^3\Sigma^-) = 2.009 \pm 0.020$ eV. Photodetachment of $HCCN^-$ to HCCN $\tilde{X}\,^3\Sigma^-$ shows a 0.4 eV long vibrational progression in ν_5, the H–CCN bending mode; the $HCCN^-$ photoelectron spectra reveal excitations up to 10 quanta in ν_5. The term energies for the excited singlet state are found to be T_0(HCCN $\tilde{a}\,^1A') = 0.515 \pm 0.016$ eV and T_0(DCCN $\tilde{a}\,^1A') = 0.518 \pm 0.027$ eV. For the isocyanocarbene, the two lowest states switch and HCNC has a singlet ground state and an excited triplet state. The electron affinities are EA(HCNC $\tilde{X}\,^1A') = 1.883 \pm 0.013$ eV and EA($\tilde{X}\,^1A'$ DCNC) $= 1.877 \pm 0.010$ eV. The term energy for the excited triplet state is T_0(HCNC $\tilde{a}\,^3A'') = 0.050 \pm 0.028$ eV and T_0(DCNC $\tilde{a}\,^3A'') = 0.063 \pm 0.030$ eV. Proton transfer kinetics in a flowing afterglow apparatus were used to re-measure the enthalpy of deprotonation of CH_3NC to be $\Delta_{acid}H_{298}(CH_3NC) = 383.6 \pm 0.6$ kcal mol^{-1}. The acidity/EA thermodynamic cycle was used to deduce D_0(H–CHCN) $= 104 \pm 2$ kcal mol^{-1} [$\Delta_f H_0$(HCCN) $= 110 \pm 4$ kcal mol^{-1}] and D_0(H–CHNC) $= 106 \pm 4$ kcal mol^{-1} [$\Delta_f H_0$(HCNC) $= 133 \pm 5$ kcal mol^{-1}]. © *2002 American Institute of Physics.* [DOI: 10.1063/1.1496473]

I. INTRODUCTION

Cyanocarbene, HCCN, is an unusual molecule. Over the last 10 years many spectroscopic studies and electronic structure calculations have clearly established that this interesting diradical is a quasilinear molecule. High resolution infrared absorption spectra[1–5] of the H–CCN bend *via* combination bands with the H–CCN stretch as well as a millimeter wavelength study[6] of the pure rotational transitions clearly establish HCCN as a semirigid bender. The infrared spectra of the combination bands of HCCN reported[4] a value for the pure H–CCN bend of 128.907 ± 0.002 cm^{-1}. Quite recently[7] far infrared laser magnetic resonance spectroscopy has been used to observe this low frequency bend at 128.907 968 7(40) cm^{-1}.

In this paper we report the photoelectron spectra of the cyanocarbene anion, $HCCN^-$, and its isomer the isocyanocarbene anion, $HCNC^-$ and obtain the electron affinities, EA(HCCN) and EA(HCNC). The $HCCN^-$ spectra show photodetachment to $\tilde{X}\,^3A''$ HCCN with a long progression

[a)]Electronic mail: nimlosm@tcplink.nrel.gov
[b)]Present address: Department of Chemistry, University of Idaho, Moscow, ID 83844-2343. Electronic mail: davico@uidaho.edu
[c)]Present address: Department of Chemistry, Purdue University, West Lafayette, IN 47907-1393. Electronic mail: pgw@purdue.edu
[d)]Electronic mail: wcl@jila.colorado.edu
[e)]Electronic mail: hadad@chemistry.ohio-state.edu
[f)]Electronic mail: george@dali.chem.wesleyan.edu
[g)]Electronic mail: barney@jila.colorado.edu

(≅0.4 eV) of H–CCN bending vibrations that reveals a higher portion of the H–CCN bending potential than has hitherto been sampled.[1–7] In addition we have observed the excited singlet state, $\tilde{a}\,^1A'$ HCCN. Photoelectron spectra of the isocyanocarbene anion show that for HCNC the singlet and triplet states have reversed, $\tilde{X}\,^1A'$ HCNC and $\tilde{a}\,^3A''$ HCNC. Further experiments of the proton transfer kinetics of $HCCN^-$ and $HCNC^-$ were used to measure the gas-phase acidities of CH_2CN and CH_2NC. Together with the electron affinities, the gas phase acidities are used to establish the absolute heats of formation of the diradicals, $\Delta_f H_{298}$(HCCN) and $\Delta_f H_{298}$(HCNC).

To anticipate our photodetachment spectra, it is useful to discuss a qualitative picture of the valence of HCCN and HCNC.[8,9] These molecules are carbenes and the parent species, CH_2, is well-known to be a bent molecule. The ground state of CH_2 is $\tilde{X}\,^3B_1$ with two low-lying[10–14] singlet states; $T_0(\tilde{a}\,^1A_1 = 0.392 \pm 0.002\,\text{eV})$ and $T_0(b\,^1B_1 = 1.02 \pm 0.05\,\text{eV})$. The states of methylene have been probed by photodetachment.[15] If the ion is written as HCX^- in Eq. (1) where $X = H$, then detachment of the $CH_2^-(\tilde{X}\,^2B_1)$ anion can produce the triplet ground state $CH_2\tilde{X}\,^3B_1$ as well as $CH_2\tilde{a}\,^1A_1$; EA(CH_2) was found to be 0.652 ± 0.006 eV.

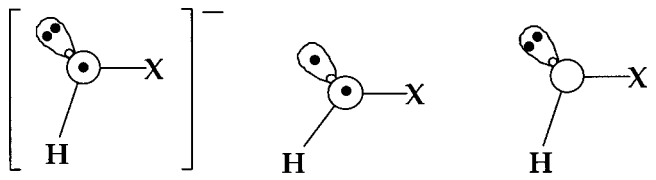

HCX^- ^3HCX ^1HCX (1)

When X=halogen, the ^{1}HCX is stabilized by back-bonding of an electron pair from the halogen X into the "empty" a'' orbital. The highly electronegative halogen atom also prefers to bond to *p*-like orbital on the carbon.[9] For the case of HCF^-, detachment of the $^2A''$ anion provides the electron affinity, EA(HCF)=0.542 ± 0.005 eV, and the photoelectron spectra[16] reveal that the HCF state ordering has switched (as predicted);[17] $\tilde{X}\,^1A'$ HCF is below $\tilde{a}\,^3A''$ HCF by 0.65 ± 0.02 eV.

It is common to regard the CN group as a *pseudo*-halogen but HCCN and HCNC will have peculiar properties that might not be anticipated by HCF or HCCℓ. By analogy to CH_2 and Eq. (1), one guesses that HCCN will be a ground state triplet and have a bent geometry, $\tilde{X}\,^3A''$. The repulsion of the H–C bonding pair of electrons with the π^2 electron pair will probably deform the CCN bond angle slightly away from 180°. Thus one would write HCCN as in Eq. (2).

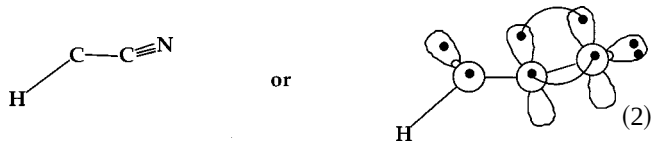

(2)

However, the π electrons of the C≡N bond are potentially able to conjugate with both electrons on the HC fragment. Consequently if the H–CCN bond angle straightens to 180°, the HCCN diradical will be stabilized[18]; the *linear* HCCN carbene becomes "doubly allylic." Consequently, unlike HCF carbene, the HCCN diradical is likely to be very floppy or quasilinear; cf. Eq. (3).

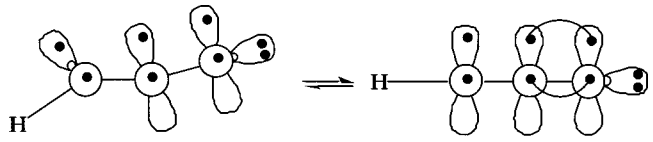

HCCN $^3A''$ HCCN $^3\Sigma^-$ (3)

Both the HCCN $^1A'$ singlet and the $HCCN^-$ $^2A''$ ion will be strongly bent, Eq. (4).

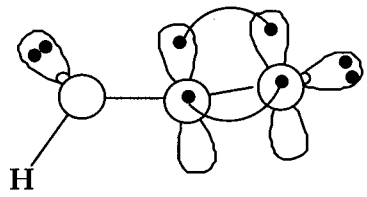

HCCN $^1A'$

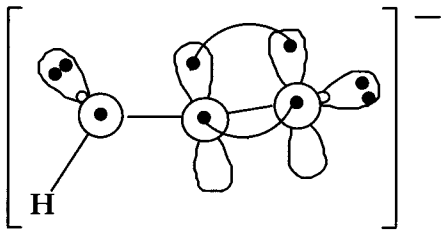

$HCCN^-$ $^2A''$ (4)

How can we describe the isomeric isocyanocarbene? If we write the GVB structure for HNC, Eq. (5), we could write analogous expressions for HCNC.

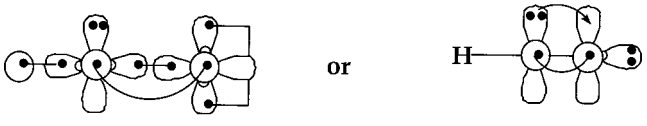

(5)

A sketch of all the states of HCCN and HCNC, together with appropriate transitions, is collected in Fig. 1. The outlines of the photoelectron spectra of $HCCN^-$ and $HCNC^-$ can now be anticipated. Photodetachment of $HCCN^-$ will produce both HCCN $^3A''$ and HCCN $^1A'$. Transitions from $HCCN^-$ to ^{3}HCCN will be characterized by extensive excitations of the H–CCN bending progression; in contrast the ^{1}HCCN state will appear as a nearly vertical band. Detachment to produce either ^{3}HCCN or ^{1}HCCN arises from different one-electron transitions; consequently one anticipates

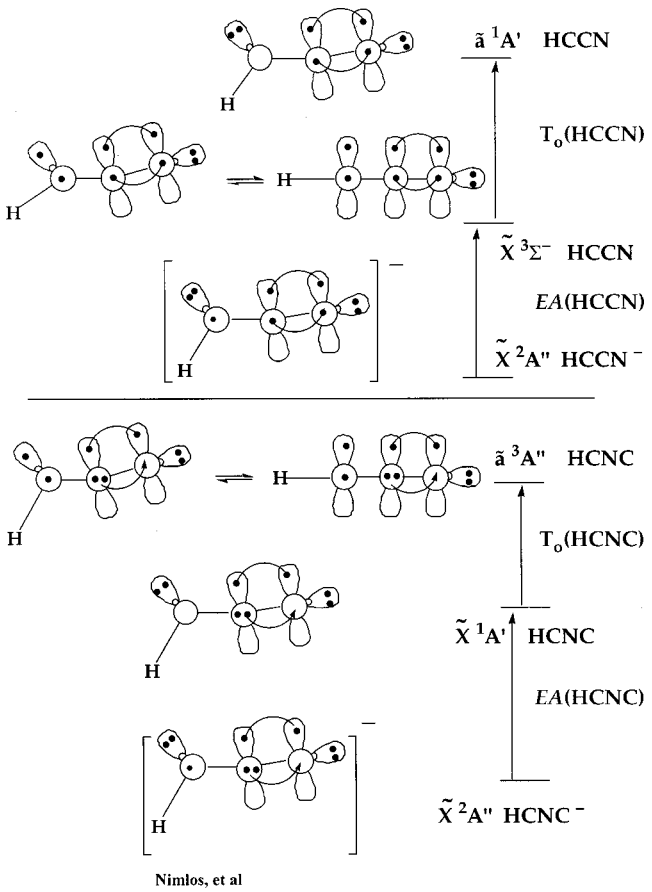

FIG. 1. Valence bond picture of states involved in photodetachment from cyanocarbene anion, $HCCN^-$ (top), and isocyanocarbene anion, $HCNC^-$ (bottom); see text for details.

different angular distributions of the scattered photoelectrons. The photodetachment of $HCNC^-$ will be similar to $HCCN^-$. We expect a pair of nearly degenerate ^{3}HCNC, ^{1}HCNC states; as in the case of cyanocarbene the ^{1}HCNC state will be more strongly bent than the triplet state and will closely resemble the geometry of the $HCNC^-$ ion.

II. EXPERIMENT

Negative ion photoelectron spectra were measured using a photodetachment apparatus described in more detail elsewhere.[15,19] Briefly, we measure the kinetic energy of electrons that are detached from a beam of mass-selected negative ions using a fixed-frequency laser. Ions are prepared in a flowing afterglow source, from which all negative ions are extracted and formed into a beam. Mass selection is achieved using a Wien mass filter and the resulting ion beam is focused into an interaction region that is located inside a ultraviolet (UV) laser build-up cavity. This cavity is pumped by a fixed frequency argon ion laser operating on either the 351.3 or 363.8 nm line. The detached electrons are collected, and their kinetic energies are measured using a hemispherical analyzer and a position sensitive detector (microchannel plate with a resistive anode). By subtracting the kinetic energy of the electrons from the energy of the laser, we obtain the electron photoelectron binding energy. Typically, the polarization of the laser is set at an angle of roughly 54.7°, the "magic angle," relative to the direction in which the electrons are collected. At this angle, the intensities of the photoelectron transitions are independent of the orbital angular momentum of the electronic transition and independent of the kinetic energy of the detached electrons. The relative intensity of the peaks in a given electronic transition is only dependent upon the Franck–Condon factors. As will be discussed below, we often change the polarization angle to help identify different electronic transitions.

The target negative ions were prepared by the reactions of acetonitrile (CH_3CN) and methylisocyanide (CH_3NC) with O^- as demonstrated by Matimba *et al.*[20,21]

$$CH_3CN + O^- \rightarrow CH_2CN \cdot OH^- \rightarrow HCCN^- + H_2O, \quad (6)$$

$$CH_3NC + O^- \rightarrow CH_2NC \cdot OH^- \rightarrow HCNC^- + H_2O. \quad (7)$$

In the photodetachment experiment, O^- ions are produced in a microwave discharge source. Roughly 0.1% O_2 is seeded in helium and passed through an Evenson microwave cavity[22] at a power of 50 W. The products from this source are then mixed with another flow of helium seeded with the CH_3CN or CH_3NC. The flow tube reactor is encased in a cooling jacket that allows the ions to be cooled to roughly 200 K by the introduction of liquid nitrogen. This cooling helps reduce the intensity of hot bands and helps simplify the photodetachment spectra. Negative ions were extracted into the beam apparatus, which is floated at +700 volts. The Wien mass filter is calibrated using O^- (m/z 16) and CH_2CN^- or CH_2NC^- (m/z 40) ions. The identities of these ions are firmly established by collecting their photodetachment spectra, which have been reported previously.[23–25] The photoelectron spectra were recorded as a function of electron kinetic energy (eKE), which is readily converted to electron binding energy (eBE) by subtracting the eKE from the laser photon energy. The absolute energy scale was fixed by the position of the $^3P_2 \leftarrow {}^2P_{3/2}$ transition in the O^- photoelectron spectrum.[25] An additional small (<1%) energy compression factor was applied as determined from the comparison of the photoelectron spectrum of the tungsten ion W^- with known transitions in tungsten atom.[26]

The flowing afterglow mass spectrometer[27] used for the gas-phase acidity measurements has been described in detail elsewhere.[28,29] All of the anions were generated by deprotonation of the appropriate precursor by either HO^- or NH_2^-. Hydroxide anion was produced by dissociative electron attachment on N_2O, followed by hydrogen-atom abstraction from CH_4. Amide NH_2^- anion was generated by dissociative electron attachment on NH_3.

Acetonitrile and acetonitrile-d_3 (Aldrich 99.95%) were used without further purification. Ultra high purity (UHP) helium (99.999%) was further purified by flowing it through a molecular sieve trap immersed in liquid nitrogen. UHP oxygen was used without further purification. Methylisocyanide (CH_3NC) was prepared by well-known chemistry.[30] Briefly, quinoline and *p*-toluenesulfonyl chloride were placed into a three-neck flask equipped with a pressure-equalizing dropping funnel, a thermometer, and a receiver trap, and cooled in liquid nitrogen, in an 8:3 molar ratio. To the solution, which was pre-heated to 75 °C and evacuated to 15 Torr, *n*-methylformamide ($HCONHCH_3$) was added drop-

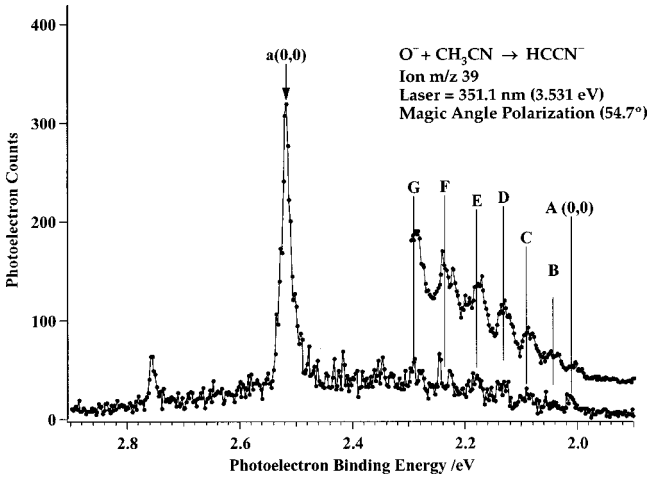

FIG. 2. The photoelectron spectrum of $HCCN^-$ where the ion is produced in a flowing afterglow source. The black connected dots show the spectrum collected with liquid nitrogen cooling of the source, while the red spectrum was collected without cooling. Peak positions are reported in Table I. Peaks **A**–**G** arise from excitation into the ^{3}HCCN while peak **a** arises from excitation into ^{1}HCCN.

wise (in a 1:4 molar ratio with respect to quinoline) to maintain a smooth distillation rate. The collected material was subsequently distilled through a Vigreux column at atmospheric pressure and used without any further purification. CD_3NC was prepared from $HCONHCD_3$ as a precursor. The purity for all samples was determined by nuclear magnetic resonance (NMR) (^{1}H and ^{13}C) and GC-MS characterizations, and acetonitrile was not present in the protiated or deuterated samples.

III. RESULTS

A. Photoelectron spectra

Figure 2 shows the photoelectron spectrum of $HCCN^-$ produced using reaction (6). There are a number of weak features in this spectrum at low energy (starting at a binding energy of 2.0 eV) and an intense feature at about 2.5 eV. Based on our discussion of the structure and bonding of the HCCN carbene, we assert that the weak features arise from the transition $\tilde{X}\,^3A''$ HCCN$\leftarrow\tilde{X}\,^2A''$ $HCCN^-$, while the sharp peak results from a photodetachment to the singlet state, $\tilde{a}\,^1A'$ HCCN$\leftarrow\tilde{X}\,^2A''$ $HCCN^-$. As mentioned above, we can cool the flowing afterglow source to about 200 K. This helps reduce spectral congestion due to hot bands and typically makes the photoelectron peaks more pronounced. The complete spectrum of $HCCN^-$ shown in Fig. 2 results from a cooled ion source. Unfortunately, cooling the source often diminishes the ion beam and consequently reduces the photoelectron signal. The insert in Fig. 2 shows the origin region of the spectrum collected at 300 K. Some features are more clearly resolved due to the increased signal level.

There is a progression of small features that we have labeled with capital letters (**A**,**B**,...) and an intense feature that we have labeled with the letter **a**. The binding energies (laser energy minus measured kinetic energy) for these peaks are collected in Table I. The small peaks arise from detachment to ^{3}HCCN and peak **a** is the origin and only peak for the transition to the ^{1}HCCN. The remaining peak in the spectrum at roughly 2.8 eV does not appear in other spectra and we have no assignment for it. The $HCCN^-$ spectrum in Fig. 2 is qualitatively similar to the photoelectron spectrum[15] observed for CH_2^-.

The lowest energy peak is identified with **A**, and we believe that the origin (0,0) of the transition to the triplet state is located within this peak, $\tilde{X}\,^3A''$ HCCN $\leftarrow\tilde{X}\,^2A''$ $HCCN^-$. The peaks identified by (**A**,**B**,...) in Fig. 2 are irregularly spaced ($\cong$350 cm^{-1}) except near the origin, where the spacings are even more complex. As mentioned in the introduction, ^{3}HCCN will have energy levels that are a mix of the H–CCN bend and rotations. However, as the energies get significantly higher than the bending barrier, the

TABLE I. Peak positions for $HCCN^-$ photoelectron spectrum.

Peak	Electron binding energy/eV	Anisotropy β	Peak spacing[a]/cm^{-1}	Assignment
A	2.014	−0.45		HCCN($\tilde{X}\,^3A''$)$\leftarrow$$HCCN^-$($\tilde{X}\,^2A''$)
				A1,$0^0\leftarrow K_a''=0,1$
			285	**A2**,$1^{\pm1}\leftarrow K_a''=2$
				A3,$1^{\pm1}\leftarrow K_a''=0,1$
B	2.050	−0.26		**B1**,$2^{\pm2}\leftarrow K_a''=2$
				B2,$2^{\pm2}\leftarrow K_a''=1$
			343	**B3**,$2^0\leftarrow K_a''=0,1$
				B4,$3^{\pm3}\leftarrow K_a''=2$
C	2.092	−0.34		**C1**,$3^{\pm1}\leftarrow K_a''=2$
			365	**C2**,$3^{\pm1}\leftarrow K_a''=0,1$
D	2.137	−0.42		**D1**,$4^{\pm2}\leftarrow K_a''=2$
				D2,$4^{\pm2}\leftarrow K_a''=1$
			362	**D3**,$4^0\leftarrow K_a''=0,1$
E	2.182	−0.39		**E1**,$5^{\pm3}\leftarrow K_a''=2$
			424	**E2**,$5^{\pm1}\leftarrow K_a''=2$
				E3,$5^{\pm1}\leftarrow K_a''=0,1$
F	2.235	−0.40	445	$6^{0,\pm2}\leftarrow K_a''=0,1,2$
G	2.290	−0.31		$7^{\pm1,\pm3}\leftarrow K_a''=0,1,2$
a	2.518±0.008	−0.77	⋯	HCCN($\tilde{a}\,^1A'$)$\leftarrow$$HCCN^-$($\tilde{X}\,^2A''$)

[a]The erratic peak splittings do not correspond to any simple mode in the HCCN molecule. As will be discussed, the ν_5(H–CCN) bending vibration is a semirigid bender and hence is a highly anharmonic mode.

molecule has harmonic levels similar to the linear molecule, $HCCN\,^3\Sigma^-$. This is what is qualitatively observed in Fig. 2.

Photoelectron angular distributions assist the assignment of the spectral features. The angular distribution of detached electrons with kinetic energy (KE), $I(\theta)$, produced by plane-polarized light has been described[31]

$$I(\theta)\approx\frac{d\sigma}{d\Omega}=\frac{\sigma_D(\mathrm{KE})}{4\pi}[1+\beta(\mathrm{KE})P_2(\cos\theta)]. \tag{8}$$

Here $\sigma_D(\mathrm{KE})$ is the total photodetachment cross section, $\beta(\mathrm{KE})$ is the anisotropy parameter, $P_2(\cos\theta)$ is the second Legendre polynomial $[\frac{1}{2}(3\cos^2\theta-1)]$, and θ is the angle between the direction of collection of detached electrons and the plane of polarization of the laser. The anisotropy factor varies between -1 and 2 depending upon the electronic transition in question. We conduct experiments in which we attempt to extract β by measuring the photoelectron spectra at $\theta=0°$ and 90°. This is accomplished by rotating a half-wave plate in the build up cavity to the appropriate angle. If we define a ratio, R=I(0°)/I(90°), the anisotropy parameter is given by Eq. (9):

$$\beta=\frac{R-1}{1+\frac{R}{2}}. \tag{9}$$

The value of β provides an important clue as to the nature of the photodetached electron. For atoms, detachment of an *s* electron leads to an outgoing *p*-wave ($\ell=1$) and $\beta=+2$, independent of the electron kinetic energy. Detachment of a *p* electron results in a mixture of interfering *s*- and *d*- waves and leads to an energy dependent value for β(E). At the photodetachment threshold, *s*-wave ($\ell=0$) detachment dominates, giving $\beta=0$ and yielding an isotropic photoelectron angular distribution. At photoelectron kinetic energies roughly 1 eV above threshold, *d*-wave detachment becomes important and $\beta\rightarrow-1$. Electron detachment from molecular ions is more complicated than the atomic case, but β is generally found to be positive for detachment for σ (*s*-like) electrons and negative for detachment for π (*p*-like) electrons.

The measurement of anisotropy factors has been successfully used to distinguish the singlet and triplet states in photodetachment spectra of other HCX^- anions.[16] In this study of the halocarbenes (HCF^-,$HCBr^-$,HCl^-), detachment to the triplet states produced a more positive β than detachment to the singlet states. Figure 1 implies that the photoelectron transition, $HCCN(\tilde{X}\,^3A'')\leftarrow HCCN^-(\tilde{X}\,^2A'')$, results from detachment of a' electrons. In contrast, the $HCCN(\tilde{a}\,^1A')\leftarrow HCCN^-(\tilde{X}\,^2A'')$ transition results from ejection of a'' electrons. It is difficult to anticipate the value of β associated with the $HCCN(\tilde{X}\,^3A'')$ or of the $HCCN(\tilde{a}\,^1A')$ value for β. Figure 1 suggests that the active a'' electron for the $HCCN(\tilde{a}\,^1A')\leftarrow HCCN^-(\tilde{X}\,^2A'')$ transition will be π-like and we anticipate a $\beta(a'')$ value of roughly -1.

Photodetachment of $HCCN^-$ with polarized laser light was used to measure the anisotropy factors for each of the HCCN features in Fig. 2. We find that the peaks

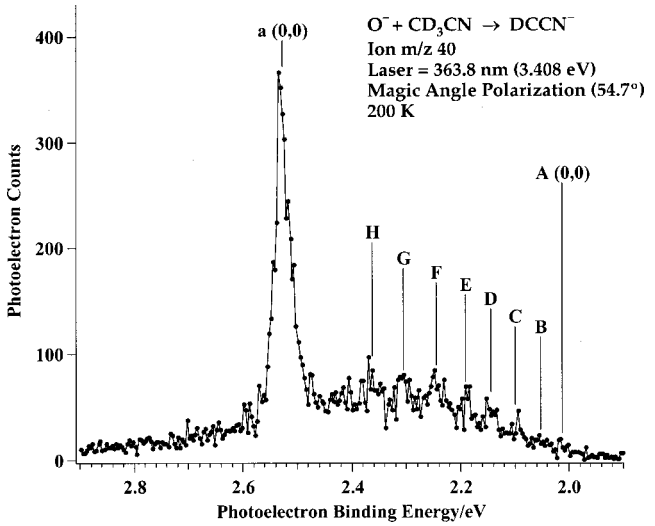

FIG. 3. The photoelectron spectrum of $DCCN^-$; the peak positions and anisotropies are reported in Table II.

labeled with (**A**,**B**,...) have different anisotropy factors $[\beta(\mathbf{A}),\beta(\mathbf{B}),...\beta(\mathbf{F})\cong-0.3]$ than the peak labeled **a**, $\beta(\mathbf{a})=-0.77$.

Figure 3 is a plot of the photoelectron spectrum of the deuterated cyanocarbene anion $DCCN^-$ and it is apparent that this spectrum is similar to $HCCN^-$. The peak positions and anisotropy factors, β, for the photoelectron spectrum of $DCCN^-$ are collected in Table II.

The photoelectron spectroscopy of isocyanocarbene anion $HCNC^-$ is similar to $HCCN^-$ in many respects. Sharp, intense features are superimposed upon weaker features that are more poorly resolved. Figure 4 shows the photoelectron spectrum of $HCNC^-$ and peak positions (**A**,**B**,**a**,**b**,...,**h**) are collected in Table III. Figure 5 is the angular distributions of $HCNC^-$ with the laser polarized at 0° and 90°. As anticipated by Fig. 1, the photoelectron spectra of $HCNC^-$ reveal the presence of two closely spaced electronic states in HCNC. The intense features **A** and **B** blend into the weak progression, (**a**,**b**,...,**h**). The β(**A**) value of -0.74 suggests detachment of a π-like a'' electron from $HCNC^-$. Consequently we assign features **A** and **B** to the singlet carbene, $HCNC(\tilde{X}\,^1A')\leftarrow HCNC^-(\tilde{X}\,^2A'')$ by their angular distribution and because of the strongly vertical nature of the transition. The weak features (**a**,**b**,...,**h**), with $\beta\cong0$, then belong to the triplet carbene, $HCNC(\tilde{a}\,^3A'')\leftarrow HCNC^-(\tilde{X}\,^2A'')$. The intervals (**a**,**b**,...,**h**) are spaced at roughly 300 cm^{-1}; this is suggestive of a progression in a low frequency bend. Figure 6 plots the photoelectron spectrum of $DCNC^-$ and the peak positions are collected in Table IV. The peak labeled **A** in Fig. 6 is close in energy to the corresponding peak in the $HCNC^-$ spectrum, confirming this as the origin of the transition to the singlet state, $HCNC(\tilde{X}\,^1A')\leftarrow HCNC^-(\tilde{X}\,^2A'')$. However, the peak labeled **a** in the $DCNC^-$ spectrum is shifted by roughly 0.042 eV from peak **a** in the $HCNC^-$ spectrum. The isotope shift implies that the

TABLE II. Peak positions for $DCCN^-$ photoelectron spectrum.

Peak	Electron binding energy/eV	Anisotropy β	Spacing[a]/cm^{-1}	Assignment
A	2.013	−0.36		$DCCN(\tilde{X}\,^3A'')\leftarrow DCCN^-(\tilde{X}\,^2A'')$
			316	**A1**, $0^0\leftarrow K_a''=0,1$ **A2**, $1^{\pm1}\leftarrow K_a''=2$
				A3, $1^{\pm1}\leftarrow K_a''=0,1$ **A4**, $2^{\pm2}\leftarrow K_a''=3$
				A5, $2^{\pm2}\leftarrow K_a''=2$ **A6**, $2^{\pm2}\leftarrow K_a''=1$
B	2.052	−0.34		**B1**, $2^0\leftarrow K_a''=0,1$ **B2**, $3^{\pm1}\leftarrow K_a''=2$
			377	**B3**, $3^{\pm1}\leftarrow K_a''=0,1$
C	2.099	−0.33		**C1**, $4^{\pm2}\leftarrow K_a''=3$ **C2**, $4^{\pm2}\leftarrow K_a''=2$
			375	**C3**, $4^{\pm2}\leftarrow K_a''=1$ **C4**, $4^0\leftarrow K_a''=0,1$
				C5, $5^{\pm3}\leftarrow K_a''=2$
D	2.145	−0.36		**D1**, $5^{\pm2}\leftarrow K_a''=2$ **D2**, $5^{\pm1}\leftarrow K_a''=0,1$
			373	**D3**, $6^{\pm4}\leftarrow K_a''=3$ **D4**, $6^{\pm2}\leftarrow K_a''=3$
				D5, $6^{\pm2}\leftarrow K_a''=2$ **D6**, $6^{\pm2}$, $6^{\pm0}\leftarrow K_a''=0,1$
E	2.191	−0.29		**E1**, $7^{\pm3}\leftarrow K_a''=2$ **E2**, $7^{\pm1}\leftarrow K_a''=2$
			436	**E3**, $7^{\pm1}\leftarrow K_a''=0,1$
F	2.245	−0.34		**F1**, $8^{\pm2}\leftarrow K_a''=2$ **F2**, $8^{\pm2}\leftarrow K_a''=2$
			487	**F3**, $8^{\pm2}$, $8^0\leftarrow K_a''=0,1$ **F4**, $9^{\pm3}\leftarrow K_a''=3$
				F5, $9^{\pm3}\leftarrow K_a''=0,1$ **F6**, $9^{\pm1}\leftarrow K_a''=2$
G	2.306	−0.37		$10^{0,\pm2}\leftarrow K_a''=0,1$
			461	
H	2.363	−0.24		$11^{\pm1}$, $12^{0,\pm2}\leftarrow K_a''=0,1$
a	2.527±0.018	−0.78		$DCCN(\tilde{a}\,^1A')\leftarrow DCCN^-(\tilde{X}\,^2A'')$

[a]The erratic peak splittings do not correspond to any simple mode in the DCCN molecule. As will be discussed, the ν_5(D–CCN) bending vibration is a semirigid bender and hence is a highly anharmonic mode.

(**a**,**b**,...,**h**) progression arises from excitation in the $(\tilde{a}\,^3A'')$ H–C–NC bend.

B. Electronic structure calculations

Tables V (HCCN) and VI (HCNC) collect the results of the electronic structure calculations[32,33] (CBS-APNO and CBS-QB3) of the negative ion and two electronic states for these species using GAUSSIAN 98.[34] The vibrational frequencies were calculated by the DFT method, B3LYP/6-311G(d,p), while the bond lengths and bond angles were the result of a QCISD/6-311G(d,p) calculation.

The electronic structure calculations in Table V reflect the qualitative notions of valence for the HCCN carbene in Eqs. (3) and (4). We have computed the barrier to linearity for each of these species (CBS-QB3). As Eq. (3) anticipates, there is a low barrier for the triplet carbene; the calculated [QCISD/6-311G(d,p)] $\Delta E(^3A'',^3\Sigma^-)$ barrier is only 275 cm^{-1}. However, these barriers are much higher for the $\tilde{X}\,^2A''$ $HCCN^-$ ion (5450 cm^{-1}) and the singlet carbene $\tilde{a}\,^1A'$ HCCN (5480 cm^{-1}). A section of the ^{3}HCCN bending curve is plotted in Fig. 7. The curve and the 275 cm^{-1} barrier result from a CBS-QB3 electronic structure calculation[33] while the HCCN bending vibrational levels are experimental values.[4,5,7] The calculations in Table V are similar to many other electronic structure calculations and experimental measurements. Four different spectroscopic (microwave[6] and

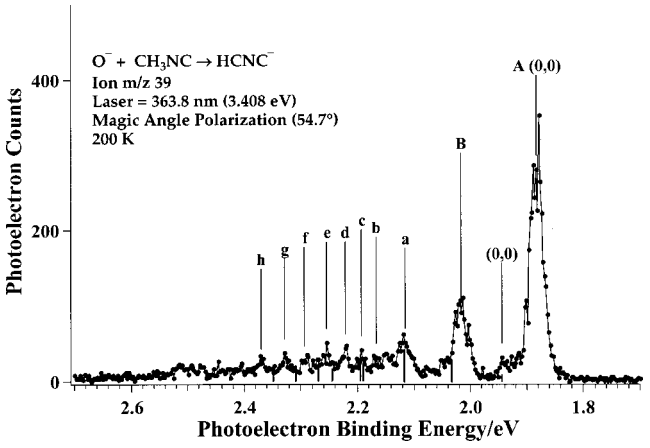

FIG. 4. The photoelectron spectrum of $HCNC^-$ produced in a flowing afterglow source. Peak positions are collected in Table III. Peaks **A** and **B** arise from excitation to ^{1}HCNC state and the peaks **a**–**h** arise from excitation to ^{3}HCNC. The bars are the results of a Franck–Condon fit to the calculated potential energy curve in the H–CNC bend in the triplet state. The origin of $\tilde{a}\,^3A''$ HCNC is identified by the (0,0) symbol and is based on the polarization data in Fig. 5 and the isotope shift in Fig. 6.

TABLE III. Peak positions for $HCNC^-$ photoelectron spectrum.

Peak	Electron binding energy/eV	Anisotropy β	Relative energy/cm^{-1}	Peak spacing/cm^{-1}
A	1.884±0.013	−0.74	0	
B	2.019±0.020	−0.48	1089	1089
C	2.151±0.017	−0.29	2156	1067
a	2.119	−0.06	1894	
b	2.167	−0.10	2279	385
c	2.194	−0.02	2501	222
d	2.219	0.03	2703	202
e	2.254	−0.10	2983	280
f	2.294	−0.01	3310	327
g	2.329	0.07	3590	280
h	2.369	−0.06	3915	325

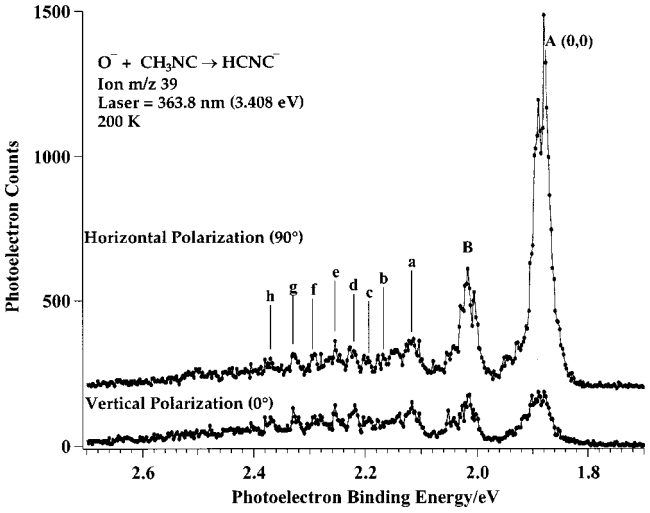

FIG. 5. The polarization dependence of the photoelectron spectrum of $HCNC^-$ where θ is the angle between the laser polarization vector and the photoelectron collection direction.

infrared[3–5]) techniques place the ^{3}HCCN barrier to linearity in the range 200–300 cm^{-1}.

The parameters for HCNC and $HCNC^-$ resemble our estimates for the isocyanocarbene in Fig. 1; α_e(H–C–NC) for $\tilde{a}\,^3A''$ HCNC is calculated to be 138° while $\tilde{X}\,^1A'$ HCNC and $\tilde{X}\,^2A''$ $HCNC^-$ have an α_e(H–C–NC) angle of roughly 104°, but the CBS-QB3 $\Delta E(^3A'', ^3\Sigma^-)$ barrier for HCNC is calculated to be 2690 cm^{-1}, so ^{3}HCNC is not nearly as ''floppy'' as ^{3}HCCN. A qualitative result of these electronic structure calculations is that $HCCN^-$, ^{1}HCCN, $HCNC^-$, ^{1}HCNC, and ^{3}HCNC will all be well-behaved molecules. However, ^{3}HCCN is a semirigid bender and will be an exceptional molecule.[35,36] The low-frequency H–CCN bending mode that is active in Eq. (3) will be an unusual vibration. The vibrational angular momentum of this low-frequency π mode will mix with the rotational angular momentum.

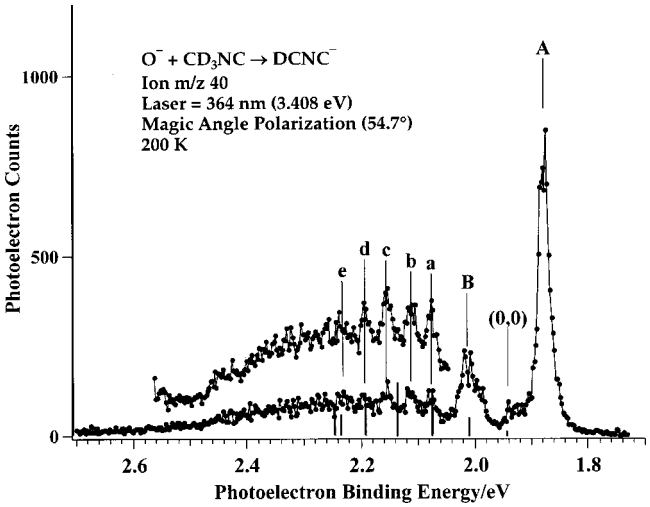

FIG. 6. The photoelectron spectrum of $DCNC^-$. The inset is a scan over a small region so as to increase signal to noise. The sticks are the results of a Franck–Condon calculation.

TABLE IV. Peak positions for $DCNC^-$ photoelectron spectrum.

Peak	Electron binding energy (eV)	Relative energy (cm^{-1})	Peak spacing (cm^{-1})
A	1.878±0.010	0	
B	2.012±0.015	1082	1082
a	2.077	1611	
b	2.113	1898	286
c	2.156	2245	348
d	2.194	2550	305
e	2.232	2856	306

We anticipate that the computed molecular properties of Tables V and VI will be reliable for all the states of HCCN and HCNC except for ^{3}HCCN. Because the ^{3}HCCN is a semirigid bender, none of the B3LYP-calculated bending frequencies nor the *A* rotational constant will be correct. As shown in Table V, the measured *A* rotational constant[6] is nearly a factor of 3 larger than the B3LYP/6-311G(*d*,*p*) value. Because of the low bent/linear barrier and the fact that the H–CCN bending mode is a semirigid bender (*vide infra*), we will treat the ^{3}HCCN molecule as if it were effectively linear, but most of the geometrical parameters for $^3A''$ HCCN (bond lengths, bond angles) in Table V, as well as all of the stretching vibrational frequencies, we expect to be reasonable values. Indeed, Table V indicates that the $^3A''$ HCCN stretching vibrations are calculated to be correct within ±4% of the measured frequencies.

C. Gas-phase ion chemistry of CH_3CN and CH_3NC

The gas phase acidity is defined[37] as the free energy required to remove a proton from a molecule. For isocyanomethane the gas-phase acidity is the $\Delta_{rxn}G_{298}$ of the following reaction:

$$CH_3NC \rightarrow CH_2NC^- + H^+. \tag{10}$$

Because of a discrepancy in the experimental gas-phase acidity of CH_3NC,[20,38] we decided to remeasure this value, being careful to insure that contamination from CH_3CN was minimal. We used a flowing afterglow device and selected-ion flow tube apparatus (SIFT) to obtain the acidity of CH_3NC by measuring the forward and reverse rate coefficients, k_{11} and k_{-11}, for proton transfer to another base. For example, k_{11} was measured for the following reaction with methoxide anion by changing the residence time in the flow tube reactor and measuring the signal for m/z 40 CH_2NC^- and m/z 31 CH_3O^-:

$$CH_3NC + CH_3O^- \rightleftarrows CH_2NC^- + CH_3OH. \tag{11}$$

The ratio of forward to reverse rate coefficients of proton transfer yields the equilibrium constant, K_{eq}, for proton transfer between methylisocyanide and the known standard, which can then be used to calculate $\Delta_{rxn}G_{298}(11)$

$$\Delta_{rxn}G_{298}(11) = -RT\ln(k_{11}/k_{-11}) = \Delta_{acid}G_{298}(CH_3OH) - \Delta_{acid}G_{298}(CH_3NC). \tag{12}$$

TABLE V. Calculated [QCISD/6-311G(d,p)] molecular geometries.

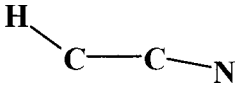

Structural parameter	$HCCN^-\cdot\tilde{X}\,^2A''$	$HCCN\,\tilde{X}\,^3A''$	$\tilde{X}\,^3A''\,\mu$wave[6]	$HCCN\,\tilde{a}\,^1A'$
r_e(H–CCN)	1.113 Å	1.078 Å		1.106 Å
r_e(HC–CN)	1.402 Å	1.339 Å		1.410 Å
r_e(HCC≡N)	1.193 Å	1.195 Å		1.177 Å
α_e(H–C–CN)	106.7°	143.1°		107.1°
α_e(HC–C–N)	173.5°	175.3°		172.8°
CBS-QB3				
ΔE(bent, linear) barrier	5450 cm^{-1}	275 cm^{-1}		5480 cm^{-1}
Rotational constants/cm^{-1}				
A	16.77	50.61	[145.100 cm^{-1}]	17.03
B	0.36	0.36	[0.368 cm^{-1}]	0.36
C	0.35	0.36	[0.365 cm^{-1}]	0.36

$\tilde{X}\,^2A''$ $HCCN^-$ B3LYP/6-311G(d,p) Harmonic modes (unscaled)

Mode	Description	Symmetry	$HCCN^-$	$DCCN^-$
ω_1	H–CCN stretch	a'	2926	2152
ω_2	HC–C≡N asym stretch	a'	1948	1940
ω_3	HC–CN stretch	a'	1072	1047
ω_4	H–C–CN bend	a'	947	794
ω_5	HC–C≡N bend	a'	512	457
ω_6	HC–C≡N bend	a''	508	503

$\tilde{X}\,^3A''$ HCCN B3LYP/6-311G(d,p) Harmonic modes (unscaled) [Ar matrix IR Refs. 45, 61, and 67]

Mode	Description	Symmetry	HCCN	Matrix IR	DCCN	Matrix IR
ω_1	H–CCN stretch	a'	3363	[3229.2 ν_1]	2500	[2424.0 ν_1]
ω_2	HC–C≡N asym stretch	a'	1796	[1734.9 ν_2]	1787	[1729.0 ν_2]
ω_3	HC–C≡N sym stretch	a'	1228	[1178.6 ν_3]	1188	[1149.2 ν_3]
ω_4	H–C–C≡N out-phase bend	a'	521	⋯	495	⋯
ω_5	H–C–C≡N in-phase bend	a'	406	⋯	332	⋯
ω_6	HC–C≡N bend	a''	455	⋯	450	⋯

$\tilde{a}\,^1A'$ HCCN B3LYP/6-311G(d,p) Harmonic modes (unscaled)

Mode	Description	Symmetry	HCCN	DCCN
ω_1	H–CCN stretch	a'	3068	2260
ω_2	HC–C≡N asym stretch	a'	2094	2085
ω_3	HC–C≡N sym stretch	a'	1091	1056
ω_4	H–C–CN bend	a'	937	773
ω_5	HC–C≡N bend	a'	461	420
ω_6	HC–C≡N bend	a''	328	321

We extracted the gas-phase enthalpy of deprotonation for CH_3NC, $\Delta_{acid}H_{298}(CH_3NC)$ from the experimental $\Delta_{acid}G_{298}(CH_3NC)$ and the calculated[32] $\Delta_{acid}S_{298}(CH_3NC)$

$$\Delta_{acid}H_{298}(CH_3NC)=\Delta_{acid}G_{298}(CH_3NC)+T\Delta_{acid}S_{298}(CH_3NC). \quad (13)$$

In Table VII, rate coefficients for the forward and reverse proton transfer reactions are provided with both methanol and ethanol as reagents. The CH_2NC^- ion was verified to be free of contamination of CH_2CN^- (<3%) via a subsequent reaction with CH_3SSCH_3. From control experiments, CH_2CN^- generates both CH_3SCHCN^- and CH_3S^- upon reaction with CH_3SSCH_3; however, CH_2NC^- generates only CH_3S^-. Using this diagnostic probe, the purity of the CH_2NC^- signal could be verified to contain less than 3% of CH_2CN^- as an impurity in the m/z 40 ion signal.

Using the literature values[39,40] for the acidity of methanol and ethanol [$\Delta_{acid}G_{298}(CH_3OH)=375.1\pm0.6$ kcal mol^{-1} and $\Delta_{acid}G_{298}(CH_3CH_2OH)=372.0\pm0.6$ kcal mol^{-1}], the gas-phase enthalpy of deprotonation of isocyanomethane [$\Delta_{acid}H_{298}(CH_3NC)$] determined in a flowing afterglow using Eqs. (10) and (11) is 383.6 ± 0.6 and 381.7 ± 0.6 kcal mol^{-1} for reactions with methanol and ethanol, respectively. These values are higher than the earliest reported[38] $\Delta_{acid}H_{298}$ value, but are in good agreement with more recent Fourier transform mass spectrometer (FTMS) experiments by Nibbering and co-workers[20] [$\Delta_{acid}H_{298}(CH_3NC)=379.8\pm2$ kcal mol^{-1}].

For the forward and reverse rate measurements in the flowing afterglow, CH_2NC^-, CH_3O^-, and $CH_3CH_2O^-$ were formed by OH^- deprotonation of CH_3NC and ROH, respectively. This prior deprotonation and the presence of excess

TABLE VI. Calculated [QCISD/6-311G(d,p)] molecular geometries.

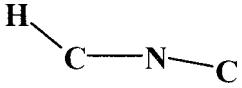

	$\tilde{X}\,^2A''$ $HCNC^-$	$\tilde{X}\,^1A'$ HCNC	$\tilde{a}\,^3A''$ HCNC
r_e(C–H)	1.124 Å	1.111 Å	1.085 Å
r_e(C–N)	1.394 Å	1.339 Å	1.309 Å
r_e(C≡N)	1.195 Å	1.202 Å	1.211 Å
α_e(H–C–NC)	102.7°	105.2°	138.2°
α_e(HC–N–C)	173.1°	171.6°	161.4°
CBS-QB3			
ΔE(bent, linear) barrier	12 100 cm^{-1}	9070 cm^{-1}	2690 cm^{-1}
Rotational constants/cm^{-1}			
A	15.66	16.44	28.06
B	0.39	0.41	0.40
C	0.38	0.40	0.40

$\tilde{X}\,^2A''$ $HCNC^-$ B3LYP/6-311G(d,p) Harmonic modes (unscaled)

Mode	Description	Symmetry	$HCNC^-$	$DCNC^-$
ω_1	H–CNC stretch	a'	2745	2012
ω_2	HC–C≡N asym stretch	a'	1870	1865
ω_3	H–C–NC bend	a'	1197	920
ω_4	HC–NC stretch	a'	969	972
ω_5	HC–N–C bend	a'	444	421
ω_6	HC–N–C bend	a''	444	438

$\tilde{X}\,^1A'$ HCNC B3LYP/6-311G(d,p) Harmonic modes (unscaled) [Ar matrix IR Ref. 61]

Mode	Description	Symmetry	HCNC	Matrix IR	DCNC	Matrix IR
ω_1	H–CNC stretch	a'	2948	[2834.5 ν_1]	2165	[2110.9 ν_1]
ω_2	HC–N≡C asym stretch	a'	1938	[1859.5 ν_2]	1930	[1856.4 ν_2]
ω_3	H–C–NC bend	a'	1202	[1173.5 ν_3]	918	[1082.9 ν_3]
ω_4	HC–NC stretch □ HC–N□C bend	a'	1120	[1080.5 ν_4]	1128	[904.5 ν_4]
ω_5	HC–N≡C bend	a'	402	···	382	···
ω_6	HC–N≡C bend	a''	267	···	261	···

$\tilde{a}\,^3A''$ HCNC B3LYP/6-311G(d,p) Harmonic modes (unscaled)

Mode	Description	Symmetry	HCNC	DCNC
ω_1	H–CNC stretch	a'	3262	2424
ω_2	HC–N≡C asym stretch	a'	1711	1704
ω_3	HC–N≡C sym stretch	a'	1257	1216
ω_4	H–C–NC bend	a'	639	507
ω_5	HC–N≡C bend	a'	395	375
ω_6	H–C–NC bend⊕HC–N≡C bend	a''	300	337

neutrals could lead to an incorrect value of the rate coefficient for each of these reactions. Therefore, we have also determined the equilibrium constant in a selected ion flow tube (SIFT), where measurements of the CH_3NC acidity *via* forward and reverse rate coefficients with CH_3OH yielded $\Delta_{acid}H_{298}(CH_3NC)$ as 383.6 ± 0.6 kcal mol^{-1}. This result is compatible with the flowing afterglow methanol value, but outside our error limits for ethanol. It is likely that competing reactions in the flowing afterglow produce an erroneous value for ethanol. Therefore, we report the enthalpy of deprotonation of CH_3NC to be $\Delta_{acid}H_{298}(CH_3NC)=383.6\pm0.6$ kcal mol^{-1}. This experimental value is in good agreement with the G2 *ab initio* electronic structure calculation[41] for $\Delta_{acid}H_{298}(CH_3NC)$ of 383.6 kcal mol^{-1} and the CBS-APNO value of 383.3 kcal mol^{-1}.

In addition to the parent compounds, the acidities of the CH_2CN and CH_2NC radicals have been established.[20] Proton-transfer studies by Nibbering and co-workers in an FTMS have bracketed the gas-phase acidities for these two radicals. Using the difference between the acidities of the reference compounds and the uncertainty in the acidities for the reference compounds,[42] the following enthalpies of deprotonation are obtained: $\Delta_{acid}H_{298}(CH_2CN)=373.6\pm3.0$ kcal mol^{-1} and $\Delta_{acid}H_{298}(CH_2NC)=378.1\pm3.8$ kcal mol^{-1}.

IV. DISCUSSION

A. Qualitatively assigned photoelectron spectra

Both HCCN and DCCN have been carefully studied earlier. Both electron paramagnetic resonance (EPR) spectroscopy[43,44] and a matrix infrared (IR) study[45] concluded that the carbene was a linear triplet, $\tilde{X}\,^3\Sigma^-$. However, beginning in 1979 a string of electronic structure calcula-

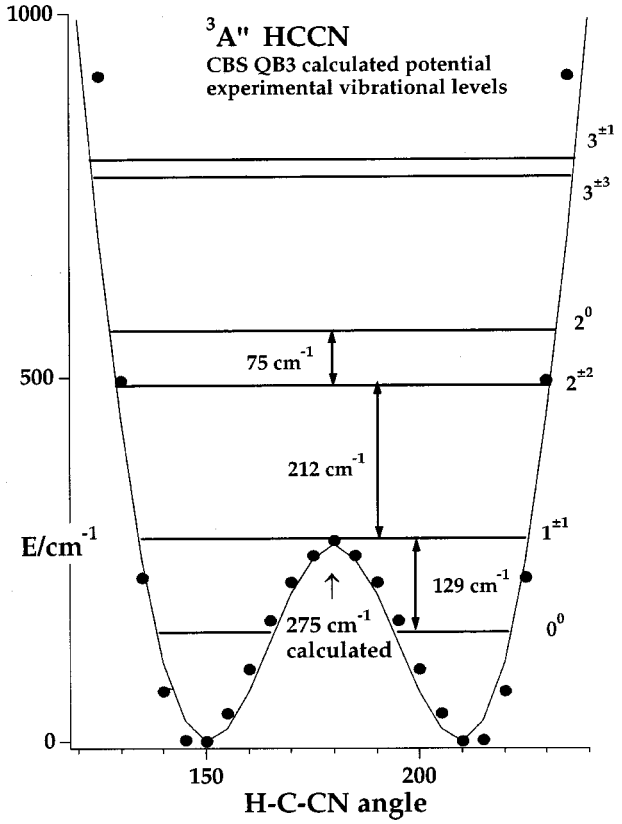

FIG. 7. The H–CCN bending potential resulting from a CBS QB3 electronic structure calculation; the vibrational levels are the result of high resolution infrared absorption spectroscopy (Refs. 4, 5, and 7).

tions[46–51] concluded that the HCCN molecule was bent with a small barrier to linearity of 300–600 cm^{-1}. These early calculations[46,50] labeled the HCCN carbene as quasilinear. A study of the rotational transitions[6] provided experimental evidence that HCCN is a semirigid bender.[35,36] Finally, high-resolution IR spectra[1–5] of the H–CCN bend *via* combination bands with the H–CCN stretch have shown that this a low-frequency mode, 128.907 ± 0.002 cm^{-1}. Low-molecular weight resist (LMR) spectra[7] of the H–CCN bending fundamental have observed this mode directly at 128.907 968 7(40) cm^{-1}.

The $HCCN^-$ photoelectron spectra reflect detachment from a strongly bent anion to a quasilinear triplet, $\tilde{X}\,^3A''$ HCCN, and a bent singlet, $\tilde{a}\,^1A'$ HCCN. Because of the low ΔE(bent, linear) barrier for ^{3}HCCN plotted in Fig. 7, we will treat the HCCN vibrational manifold as if HCCN were $^3\Sigma^-$ and effectively linear. Table VIII provides a correlation between the six vibrational modes of $^3A''$ HCCN (bent) and $^3\Sigma^-$ HCCN (linear). The $HCCN^-$ spectra in Fig. 2 show detachment to a pair of different electronic states of HCCN. The first state is surely the $\tilde{X}\,^3\Sigma^-$ HCCN, which features a long progression in an irregular bending progression (**A**, **B**, **C**, **D**, **E**, **F**, and **G**); see Table I. Feature **a** in Fig. 2 is assigned as the origin of the $\tilde{a}\,^1A'$ HCCN. As predicted by the generalized valence band (GVB) structures in Fig. 1, the large structural change between the bent $\tilde{X}\,^2A''$ $HCCN^-$ and the quasilinear $\tilde{X}\,^3\Sigma^-$ HCCN is reflected in the 0.4 eV long Franck–Condon profile. The small change in geometry between the $HCCN^-$ and ^{1}HCCN results in a single intense feature **a** that marks the origin for the $\tilde{a}\,^1A'$ HCCN $\leftarrow\tilde{X}\,^2A''$ $HCCN^-$ transition. The measured angular distributions (Fig. 3) reported in Table I clearly distinguish the long progression of the $\tilde{X}\,^3\Sigma^-$ HCCN state ($\beta \cong -0.3$) from the intense **a** feature that marks the $\tilde{a}\,^1A'$ HCCN state ($\beta \cong -0.8$).

To locate the origin of the triplet transition, $\tilde{X}\,^3\Sigma^-$ HCCN, in Fig. 2 we rely upon the measurements at different flow tube temperatures, isotope studies, semirigid bender calculations, and electronic structure calculations. The HCCN feature **A** in Fig. 2 appears to be the lowest energy transition in the spectra at both 300 K (red) and 200 K (black); see Table I. The fact that the relative intensity of this feature, centered at 2.014 eV, does not change significantly upon cooling from 300 to 200 K suggests that it is not a hot band. The first feature in the photoelectron spectrum of $DCCN^-$ (peak **A** in Fig. 4) is at nearly the same energy, 2.013 eV; see Table II. One expects the (0,0) band to experience little or no shift upon deuteration. Consequently the un-corrected or raw electron affinity obtained from the **A** peak [EA(HCCN)=2.014 eV or 46.4 kcal mol^{-1}] is close to the value calculated using CBS-APNO (46.0 kcal mol^{-1}) as shown in Table IX.

The $HCCN^-$ and $DCCN^-$ spectra in Figs. 2 and 3 are consistent with the GVB diagrams in Fig. 1. The angular distributions and Franck–Condon profiles reveal detachment from a $\tilde{X}\,^2A''$ $HCCN^-$ ion to the ground state, $\tilde{X}\,^3\Sigma^-$ HCCN, with an EA(HCCN) of about 2 eV. Detachment to the singlet state of cyanocarbene provides a term value, $T_0(\tilde{a}\,^1A'$ HCCN), of roughly 0.5 eV.

The photoelectron spectra of the $HCNC^-$ are shown in Figs. 4–6 and they are quite different from the $HCCN^-$ spectra. We associate the intense sharp peaks **A** and **B** with

TABLE VII. Flowing afterglow and SIFT rate coefficients for proton transfer between methanol, ethanol, and methylisocyanide and their conjugate bases.[a]

Reaction	$k_{FA}/10^{-10}$ cm^3 $molecule^{-1}$ s^{-1}	$k_{SIFT}/10^{-10}$ cm^3 $molecule^{-1}$ s^{-1}
$CH_2NC^- + CH_3OH \rightarrow CH_3NC + CH_3O^-$	4.7±0.9	3.8±0.5
$CH_3O^- + CH_3NC \rightarrow CH_3OH + CH_2NC^-$	3.4±0.5	3.2±0.6
$CH_2NC^- + CH_3CH_2OH \rightarrow CH_3NC + CH_3CH_2O^-$	2.5±0.1	
$CH_3CH_2O^- + CH_3NC \rightarrow CH_3CH_2OH + CH_2NC^-$	0.25±0.06	

[a]The error in the rate constant is one standard deviation of these individual rate measurements. The flowing afterglow experiments were carried in Columbus while the selected-ion flow tube measurements were done in Boulder.

TABLE VIII. Correlation of vibrational modes of ^{3}HCCN between bent ($^3A''$) and linear ($^3\Sigma^-$) structures. The $^3A''$ HCCN harmonic modes (ω) are from Table V and are unscaled; the $^3\Sigma^-$ HCCN experimental modes (ν) and are reported by matrix isolation IR spectroscopy (Refs. 45 and 61) and by far-infrared laser magnetic resonance (FIR LMR) (Ref. 7).

bent HCCN $^3A''$ [3 rotations $\oplus$6 vibs]	linear HCCN $^3\Sigma^-$ [2 rotations $\oplus$7 vibs]
a' modes	σ modes
ω_1 H–CCN stretch=3363 cm^{-1}	ν_1 H–CCN stretch=3229 cm^{-1}
ω_2 HC–C≡N asym st.=1796 cm^{-1}	ν_2 HC–C≡N asym st.=1735 cm^{-1}
ω_3 HC–C≡N sym st.=1228 cm^{-1}	ν_3 HC–C≡N sym st.=1178.5 cm^{-1}
ω_4 HC–C≡N out-phase bend=521 cm^{-1}	
ω_5 HC–C≡N in-phase bend=406 cm^{-1}	π modes
	ν_4 HC–C≡N bend=369.5 cm^{-1}
a'' modes	ν_5 H–C–CN bend=128.9 cm^{-1}
ω_6 HC–C≡N bend=455 cm^{-1}	

detachment to the $\tilde{X}\,^1A'$ HCNC; this is further confirmed by the angular distribution, $\beta(\mathbf{A})=-0.74$. There is detachment to a second electronic state of HCNC beginning near feature **a**. Because of the angular distribution of these peaks, $\beta\cong 0$, and the extended Franck–Condon profile, we assign these features to $\tilde{a}\,^3A''$ HCNC. These data are in accord with Fig. 1 and we have preliminary values for EA(HCNC) of 1.9 eV and the T_0(HCNC) of 0.2 eV.

TABLE IX. Thermochemistry: Calculated energies (in Hartree) and derived heats of formation ($\Delta_f H_{298}$), acidities ($\Delta_{acid}H_{298}$), bond dissociation energies (D_0), bond enthalpies (DH_{298}), electron affinities (EA), and term energies (T_0) in kcal mol^{-1}.

Species	CBS-ANPO (E_0 Hartree)	CBS-QB3 (E_0 Hartree)	B3LYP (E_0 Hartree)	Experimental kcal mol^{-1}	Ref.
$CH_3CN\ \tilde{X}\,^1A_1$	(−132.706 45)	(−132.526 61)	(−132.748 11)		
$CH_2CN^-\ \tilde{X}\,^1A'$	(−132.110 85)	(−131.931 37)	(−132.143 31)		
$CH_2CN\ \tilde{X}\,^2B_1$	(−132.055 15)	(−131.875 82)	(−132.100 93)		
$HCCN^-\ \tilde{X}\,^2A''$	(−131.463 82)	(−131.284 63)	(−131.498 66)		
$HCCN\ \tilde{X}\,^3A''$	(−131.390 44)	(−131.211 42)	(−131.439 91)		
$HCCN\ \tilde{a}\,^1A'$	(−131.369 47)	(−131.190 89)	(−131.431 86)		
$CH_3NC\ \tilde{X}\,^1A_1$	(−132.668 36)	(−132.488 96)	(−132.709 75)		
$CH_2NC^-\ \tilde{X}\,^1A'$	(−132.058 72)	(−131.878 93)	(−132.090 50)		
$CH_2NC\ \tilde{X}\,^2B_1$	(−132.017 55)	(−131.837 95)	(−132.063 57)		
$HCNC^-\ \tilde{X}\,^2A''$	(−131.419 77)	(−131.240 34)	(−131.454 67)		
$HCNC\ \tilde{X}\,^1A'$	(−131.349 88)	(−131.171 69)	(−131.393 98)		
$HCNC\ \tilde{a}\,^3A''$	(−131.346 96)	(−131.166 50)	(−131.396 01)		
$\Delta_f H_{298}(CH_3CN)$				15.4±1.7	68
$\Delta_{acid}H_{298}(H–CH_2CN)$	374.6	374.4	380.4	372.9±2.1	69
$D_0(H–CH_2CN)$	95.0	94.7	91.0	93±2	63
$DH_{298}(H–CH_2CN)$				95±2	63
$\Delta_f H_0(CH_2CN)$	56.3	57.2	53.5	56±3	63
$\Delta_f H_{298}(CH_2CN)$	59.8	59.5	55.8	58±3	63
$EA(CH_2CN)$	35.0	34.9	26.6	35.58±0.32	23
$\Delta_{acid}H_{298}(H–CHCN)$	371.8	371.7	378.6	373.6±3.0	23
$D_0(H–CHCN)$	103.4	103.3	99.7	104±2	this work
$\Delta_f H_0(HCCN)$	107.3	108.4	104.9	110±4	this work
EA(HCCN)	46.0	45.9	36.9	46.2±0.3	this work
$T_0(\tilde{a}\,^1A'–\tilde{X}\,^3A'')$	13.2	12.9	16.5	11.9±0.3	this work
$\Delta_f H_{298}(CH_3NC)$				39.08±1.72	65
$\Delta_{acid}H_{298}(H–CH_2NC)$	383.3	383.5	389.3	381.9±3.0	this work
$D_0(H–CH_2NC)$	94.7	94.9	90.4	91±3	this work
$DH_{298}(H–CH_2NC)$	96.3	96.4	91.9	93±3	this work
$\Delta_f H_0(CH_2NC)$	79.5	80.9	76.4	77±3	this work
$\Delta_f H_{298}(CH_2NC)$	83.3	83.3	78.8	80±4	this work
$EA(CH_2NC)$	25.8	25.7	16.9	24.42±0.55	24
$\Delta_{acid}H_{298}(H–CHNC)$	375.7	375.6	382.7	378.3±3.8	24
$D_0(H–CHNC)$	105.3	104.4	105.1	106±4	this work
$DH_{298}(H–CHNC)$	106.5	105.8	106.4	108±4	this work
$\Delta_f H_0(HCNC)$	130.6	131.1	131.7	133±5	this work
$\Delta_f H_{298}(HCNC)$	134.1	133.4	134.0	136±5	this work
EA(HCNC)	43.9	43.1	38.1	43.4±0.3	this work
$T_0(\tilde{a}\,^3A''–\tilde{X}\,^1A_1)$	1.8	3.3	−1.3	1.4±0.6	this work

B. Photoelectron assignments for HCCN and HCNC

The detailed assignment of the origin of the $HCCN^-$ is interesting because the active mode in the 4000 cm^{-1} long Franck–Condon profile is ν_5, the semirigid bender. Quasilinear molecules have been discussed in detail by Bunker[36] and Winnewisser.[52] As shown in Eq. (3) the HCCN molecule exists between a strictly bent structure, $^3A''$, and a strictly linear structure, $^3\Sigma^-$. In the bent structure with a high barrier to linearity, the H–CCN bending vibration of the molecule could be treated as a harmonic oscillator and a prolate rigid rotor, with the *a* rotational axis being roughly parallel to the CC bond. The rotation–vibrational energy for the H–CCN bend, ν_5, can be described[53] by

$$E(\nu_5,J,K_a)=h\nu_5(\nu_5+1/2) + \overline{B}J(J+1)+(A-\overline{B})K_a^2. \quad (14)$$

In Eq. (14), ν_5 is the quantum number for the bending vibration ν_5, B is the average of the *B* and *C* rotational constants, $(B+C)/2$, and is roughly 0.36 cm^{-1}, *J* is the rotational quantum number, *A* is the rotational constant, and K_a is the projection of *J* on the *a* rotational axes, $K_a \leqslant J$. For a linear carbene, $^3\Sigma^-$ HCCN, the H–CCN bending vibration is degenerate and has angular momentum, ℓ; the rotation–vibrational energy would then be written as[53]

$$E(\nu_5,J,\ell)=h\nu_5(\nu_5+1)+\overline{B}J(J+1)+g\ell^2. \quad (15)$$

There are no analytic expressions that describe the rotation–vibrational energy levels of a semi-rigid bender, although approximate Hamiltonians exist to describe high-resolution infrared absorption experiments.[54] A quasilinearity parameter, γ_0, is defined[55,56] as

$$\gamma_0 \equiv 1-4\left[\frac{E(\text{lowest state with } K_a \text{ or } \ell=1)}{E(\text{lowest excited state with } K_a \text{ or } \ell=0)}\right]. \quad (16)$$

The parameter γ_0 should lie between roughly 1 for a rigidly bent molecule and roughly -1 for a linear molecule. For HCCN, γ_0 was recently estimated to be from -0.07 to -0.33 from microwave spectroscopy experiments[6] and -0.24 from IR measurements.[4] The K_a rotational quantum number from the bent case ($HCCN\ ^3A''$) must transform into the ℓ quantum number in the linear case ($HCCN\ ^3\Sigma^-$), and the quasilinear levels can be related to these two quantum numbers. In Fig. 8 we have shown the correlation between the levels of HCCN and those for a rigidly bent molecule and a linear molecule; the dotted lines $(\cdots)$ correlate the quantum number K_a and ℓ; $K_a \leftrightarrow \ell$.

To understand the $HCCN^-$ photoelectron transitions in Fig. 2 and to find an accurate origin of the photodetachment spectra, we use Curl's semirigid bender (SRB) calculations[57] for HCCN and DCCN. As mentioned in the introduction, the vibrational intervals, $\Delta E(1\nu_5^{\pm 1},0) \cong 129\ cm^{-1}$ and $\Delta E(2\nu_5^{\pm 2},1\nu_5^{\pm 1}) \cong 213\ cm^{-1}$, have been measured for HCCN[4,5,7] as well as for ^{3}DCCN (75 and 208 cm^{-1}). Higher HCCN $n\nu_5^{\pm \ell}$ levels have been calculated by a semirigid bender program[57] (see Fig. 9). Detachment from the $\tilde{X}\,^2A''$ state of $HCCN^-$ to $\tilde{X}\,^3A''$ state of HCCN dictates that the transition moment must have a' symmetry or that the transition is a parallel one and in the plane of the HCCN molecule. As a result, the selection rule[58] for these bent/linear transitions is $\Delta K_a = 0, \pm 1$. Electronic structure calculations of ΔE(bent/linear) for $HCCN^-$ in Table V conclude that the barrier is about 5300 cm^{-1}. Consequently we treat the ion as if it were bent and we calculate the energies of the states of the negative ion using Eq. (14). At the temperatures of this experiment (200 and 300 K) there is significant population only in the $K_a''=0$, 1, and 2 states in $HCCN^-$ and $K_a''=0$, 1, 2, and 3 states in $DCCN^-$.

An expanded view of the origin of the $HCCN^-$ and $DCCN^-$ photodetachment spectra is shown in Figs. 8 and 10. This is an attempt to understand the feature **A** (0,0) in

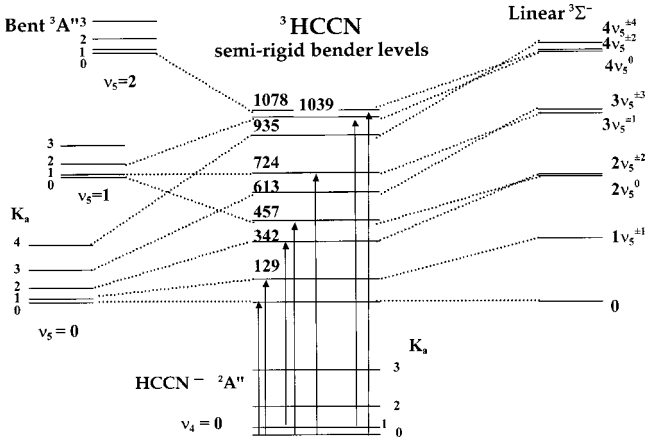

FIG. 8. An expanded view of the origin of the photoelectron spectrum of $HCCN^-$. The upper trace was measured for ions produced at room temperature, the middle was measured for ions produced in the range 200–300 K, and the lower shows ions produced at 200 K. Energies for calculated transitions are shown with arrows and identities of these are shown in Table I (see text).

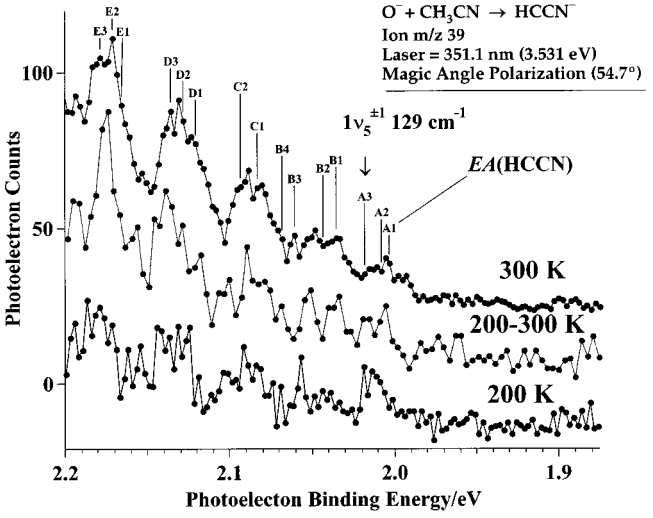

FIG. 9. A schematic picture of the H–CCN bending vibrational and rotational energy levels for a bent molecule (left) and a linear molecule (right). ^{3}HCCN is a quasilinear molecule and its vibrational–rotational levels are a complex mixture of bending and rotational levels. The correlation of each level in HCCN to bent and linear states is shown. The first three excited levels are reported in the literature (Refs. 4, 5, and 7). At higher energies the levels of HCCN will start to approximate the harmonic spacings of a linear molecule.

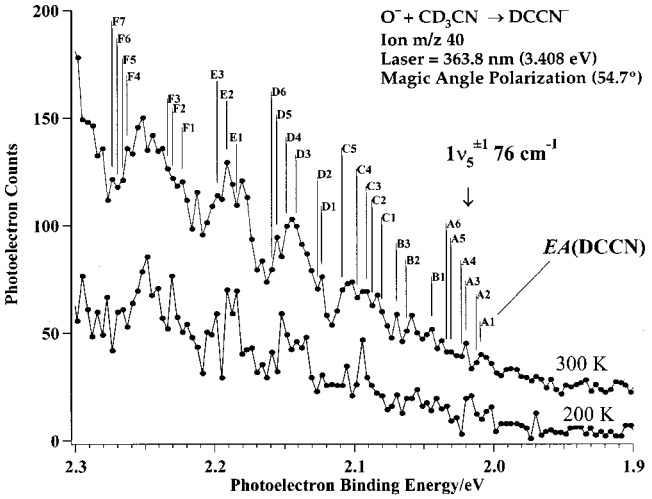

FIG. 10. An expanded view of the origin of the photoelectron spectrum of $DCCN^-$. The upper trace was collected at 300 K, the lower trace at 200 K. Energies for calculated transitions are shown with arrows and identities of these are shown in Table I (see text).

both Figs. 2 and 3. In Figs. 8 and 10 we also show the lower energy portion of the photoelectron spectra for these anions at different flow tube temperatures. Superimposed upon the photoelectron spectra are transitions predicted by the semirigid bender calculations[57] for HCCN (Fig. 8) and DCCN (Fig. 10). Each transition calculated by the SRB program is identified with a letter and number and the assignments are shown in Tables I and II. These transitions are identified by the Ka'' quantum number in the negative ion ($v_4''=0$) and the linear quantum numbers, Eq. (15), for the triplet carbene. (Tables V and VI identify ω_4 as the H–CCN bending mode in the $HCCN^-$ and $DCCN^-$.) For instance, the transition from $v_4''=0$, $K_a''=2$ in the ground state of $HCCN^-$ to $v_5'=1$, $\ell=\pm1$ in the triplet state of HCCN is marked **A2** in the spectrum and denoted $1^{\pm1}\leftarrow Ka''=2$ in Table I. This convention is used for the rest of the calculated transitions shown in Tables I and II for $HCCN^-$ and $DCCN^-$. When the splitting of two transitions is small, they are listed together on the figure. In Tables I and II we have grouped together the transitions that correspond to peaks (**A**,**B**,...) identified in Figs. 2 and 3. Feature **A3** labels the $^3\Sigma^-$ HCCN $1\nu_5^{\pm1}$ state and it is split from the (0,0) band **A1** by 129 cm^{-1}. As Figs. 8 and 10 show, the transitions calculated using the SRB program appear to bunch together roughly where the experimental photoelectron peaks are located. However, at higher energies the fit appears to break down. One would not expect very good agreement for the higher v states, since there was no input from the higher v states into the quartic potential used by the SRB. As a result, we believe that the agreement between the semirigid bender levels and the photodetachment data in Fig. 10 is actually reasonably good.

Once the origins of the photoelectron spectra of $HCCN^-$ and $DCCN^-$ are assigned, one can extract the electron affinity. The feature **A1** in Fig. 8 labeled with the transition $0^0\leftarrow K_a''=0,1$ is the origin of the $HCCN^-$ spectrum and from this we extract an electron affinity, EA(HCCN) $=2.003\pm0.014$ eV. The 14 meV error limits are chosen conservatively to encompass most of the (**A1**,**A2**,**A3**) clump in Fig. 8. For the deuterated isomer we find EA(DCCN)$=2.009\pm0.020$ eV. The 20 meV error limits cover the (**A1**,**A2**,**A3**,**A4**) clump in Fig. 10. The small shift in EA(HCCN) upon deuteration is consistent with the zero-point energies calculated using the vibrational frequencies in Table V.

A small correction needs to be made to the electron affinity to account for the rotational excitation in the negative ion. The final, corrected EA is extracted from the raw EA *via* this rotational correction which is commonly given by[59,60] Eq. (17)

$$\Delta_{\mathrm{rot}}\cong k_BT\left[\frac{A'}{2A''}+\frac{B'}{2B''}+\frac{C'}{2C''}-\frac{3}{2}\right]+\left(\frac{B''-B'}{3}\right), \qquad (17)$$

where k_B is the Boltzmann constant, T is the ion temperature, and A, B, and C are the rotational constants for neutral (A',B',C') and negative ion (A'',B'',C''). The expression (17) is derived assuming symmetric top rotations and harmonic vibrational modes; consequently this is a valid approach for the $HCNC^-$ ion but is suspect for $HCCN^-$ since ^{3}HCCN is a quasilinear species. However, the SRB calculations[57] explicitly deal with the rotational–vibrational congestion so we do not have to employ Eq. (17) to make a large rotational correction to the raw electron affinity. The final, corrected electron affinities are EA(HCCN)$=2.003\pm0.014$ eV and EA(DCCN)$=2.009\pm0.020$ eV.

Identification of the origin for the transition to the $\tilde{a}\,^1A'$ state is straightforward because of the vertical Franck–Condon profile and the break in the angular distribution, β. As seen in Tables I and II, the energy for the **a** feature is 2.518 ± 0.008 eV for HCCN and 2.527 ± 0.018 eV for DCCN. This fixes the term energy for the singlet state $T_0(\mathrm{HCCN}\,\tilde{a}\,^1A')=0.515\pm0.016$ eV and $T_0(\mathrm{DCCN}\,\tilde{a}\,^1A')=0.518\pm0.027$ eV.

The Franck–Condon profiles and polarization data in Figs. 4–6 establish that the ground state of HCNC is $\tilde{X}\,^1A'$. The feature **A** in Figs. 5 and 6 is the (0,0) band and furnishes us with the raw electron affinities: EA(HCNC)$=1.884\pm0.013$ eV and EA(DCCN)$=1.878\pm0.010$ eV. Using the rotational constants in Table VI and expression (17), we derive the final electron affinities for HCNC; EA(HCNC)$=1.883\pm0.013$ eV and EA(DCNC)$=1.877\pm0.010$ eV.

From the polarization data (Fig. 6 and Table VI), it is clear that peaks **A** and **B** belong to the HCNC $\tilde{X}\,^1A'$ state, while the peaks labeled with lower case letters (**a**,**b**,...) belong to the triplet carbene, HCNC $\tilde{a}\,^3A''$. We observe features **A** and **B** in Fig. 4 to be split by 1089 ± 190 cm^{-1} and a similar interval is observed for DCNC (1082 ± 170 cm^{-1}) in Fig. 6. On the basis of the harmonic frequencies in Table VI, we use ω_4 to assign **B** as one quantum of excitation of ν_4, the HC–N≡C bend. Table VI reports that the harmonic mode is calculated at 1120 cm^{-1} and ν_4 is observed in an Ar matrix at 1080.5 cm^{-1}. The electronic structure calculations of the harmonic modes of HCNC and DCNC in Table VI imply that two of the vibrational fundamentals, ν_3 and ν_4, of DCNC have been mis-assigned. The B3LYP/6-311G(p,d) calculations predict a tiny shift for ω_4, the HC–NC stretch, while ω_3, the H–C–NC bend at 1202 cm^{-1}, is expected fall

to 918 cm^{-1} in the D–C–NC isotopomer. It seems sensible for us to reassign the matrix spectra[61] for DCNC with ν_3 as 904.5 cm^{-1} and ν_4 at 1082.9 cm^{-1}.

Identification of the origin of the transition HCNC $\tilde{a}\,^3A'' \leftarrow$ HCNC$^-$ $\tilde{X}\,^2A''$ is more difficult. We can clearly identify peaks **a**–**h** in the spectrum of both $HCCN^-$ and $DCCN^-$ as belonging to the $\tilde{a}\,^3A''$ state of HCNC. The anisotropy of these peaks (β=0.0 to −0.1) relative to those for peaks β(**A**) and β**B**) demonstrates that these features do not belong to the HCNC $\tilde{X}\,^1A'$ ground state.

Assignment of the (0,0) band for HCNC $\tilde{a}\,^3A''$ becomes complicated because the apparent origin for this transition, **a**, is shifted by 0.042 eV to the red upon deuteration. The calculated shift of the origin based upon the zero-point energies of the negative ion and the triplet state (from Table VI) is 0.003 eV. We have conducted experiments at 300 K, which suggest that peak **a** in the $DCCN^-$ spectrum is not a hot band. Thus it is likely that peak **a** in HCNC $\tilde{a}\,^3A''$ and DCNC $\tilde{a}\,^3A''$ arises from an overtone in the H–C–NC bend.

To locate the origin, we calculated the potential energy curves for the H–C–NC bend in the $HCNC^-$ and $\tilde{a}\,^3A''$ HCNC and we calculated the resultant Franck–Condon factors. We move the origin of the transition in the photoelectron spectrum for both $HCNC^-$ and $DCNC^-$ until a calculated peak matches with peak **a**. The result of our best fit is that we obtain a binding energy for the $\tilde{a}\,^3A''$ HCNC of 1.944 eV for both HCNC and DCNC; the calculated Franck–Condon factors are shown as red sticks in Figs. 4 and 6. As can be seen, there is a weak feature at this location which matches with the small calculated Franck–Condon factor for the $\tilde{a}\,^3A''$ origin. We assign this as the origin and, with the rotational correction, the binding energy is 1.933 ± 0.025 eV for HCNC and 1.925 ± 0.025 eV for DCNC. These error limits are chosen to account for the breadth of the shoulder on peak **A**, which we assign as the origin. The term energies for the triplet is $T_0(\text{HCNC}\,\tilde{a}\,^3A'') = 0.050 \pm 0.028$ eV and $T_0(\text{DCNC}\,\tilde{a}\,^3A'') = 0.063 \pm 0.030$ eV, which is close to the electronic structure calculations of Table IX; CBS-APNO value for $T_0(\text{HCNC}\,\tilde{a}\,^3A'')$ is 0.078 eV.

C. HCCN and HCNC thermochemistry

Using EA(HCCN) and EA(HCNC) and gas phase enthalpies of deprotonation, $\Delta_{acid}H_{298}$, it is now possible to complete a number of thermodynamic cycles[62,63] for CH_3CN and CH_3NC. The enthalpy of deprotonation, $\Delta_{acid}H_{298}(\text{RH} \rightarrow \text{R}^- + \text{H}^+)$, can be related to the acidity, ionization potential, and the electron affinity:

$$\Delta_{acid}H_{298}(\text{RH}) = \text{DH}_{298}(\text{RH}) + \text{IP(H)} - \text{EA(R)} - \int dT[C_p(\text{R}) - C_p(\text{R}^-) + C_p(\text{H}) - C_p(\text{H}^+)]. \quad (18a)$$

In (18a) IP(H) is the ionization potential of the hydrogen atom[26] and the integrated heat capacities (C_p) are calculated *via* equilibrium statistical mechanics.[64] Because HCCN is a semirigid bender, it will not be so straightforward to compute the integrated heat capacity of this carbene, $\int dT\, C_p(\text{HCCN})$. As shown in the Appendix, we can re-write the acidity/EA cycle as

$$\Delta_{acid}H_{298}(\text{RH}) = D_0(\text{RH}) + \text{IP(H)} - \text{EA(R)} - \int dT[C_p(\text{R}^-) + C_p(\text{H}^+) - C_p(\text{RH})]. \quad (18b)$$

Table IX collects the thermochemistry of HCCN and HCNC. The experimental C–H bond energies, DH_{298}(RH) for CH_3NC, CH_2CN, and CH_2NC, are obtained using Eqs. (18a) and (18b). Using these bond energies, we calculate the heats of formation of CH_2NC, HCCN, and HCNC from the known[65] heats of formation of the CH_3NC and CH_2CN. Table IX lists the experimental results and compares them with electronic structure calculations. The computational results are referenced to the heats of formation of CH_3CN and CH_3NC. Results for values calculated using the CBS-APNO technique are given in Table IX. This technique has been shown to have a root-mean-square (rms) error[32] of 0.7 kcal mol^{-1} for the G2 test set. For comparison, we have also calculated energies using the more recent CBS-QB3 technique.[33] This method is similar to the CBS-Q technique, but it optimizes the geometry and conducts a frequency calculation at the B3LYP/6-311G(d,p) level, and it utilizes coupled-cluster single double triple [CCSD(T)], rather than QCISD(T), for the ultimate energetic calculations. It is reported that the rms error is 1.1 kcal mol^{-1} for the G2 set,[33] but these calculations are much more efficient than the CBS-APNO method. Table IX also lists the results obtained from B3LYP/6-311G(d,p) calculations, which is even faster. As can be seen, there are only minor differences between the CBS-QB3 and CBS-APNO calculations. The B3LYP/6-311G(d,p) technique produces a greater error in energy but provides fairly accurate molecular geometries and vibrational frequencies.

Recently[66] a set of collision-induced dissociation studies of deprotonated chloroacetonitrile have been reported: $C\ell CHCN^- \rightarrow HCCN + C\ell^-$. Using a measurement of the threshold for chloride dissociation, the absolute heat of formation of the cyanocarbene and the bond energy of the cyanomethyl radical were found: $\Delta_f H_{298}(\text{HCCN}) = 115.6 \pm 5.0$ kcal mol^{-1} and $DH_{298}(\text{H–CHCN}) = 107.3 \pm 5.4$ kcal mol^{-1}. As we describe in the Appendix, the usual route the acidity/EA cycle used to find bond energies is *via* Eq. (18a), which requires $\int dT\, C_p(\text{HCCN})$. Since HCCN is a floppy molecule, the heat capacity integral is a difficult sum to perform and we have adopted Eq. (18b) instead. Consequently we cannot measure DH_{298}(H–CHCN) to compare with the CID measurement; Table IX only reports D_0(H–CHCN) value of 104 ± 2 kcal mol^{-1}.

It is always interesting to contrast the thermochemistry of (HCCN–HCNC) polyatomic radicals and Table IX provides some interesting examples in Eq. (19). For comparison we list the corresponding values[63] for CH_4 in Eq. (19a).

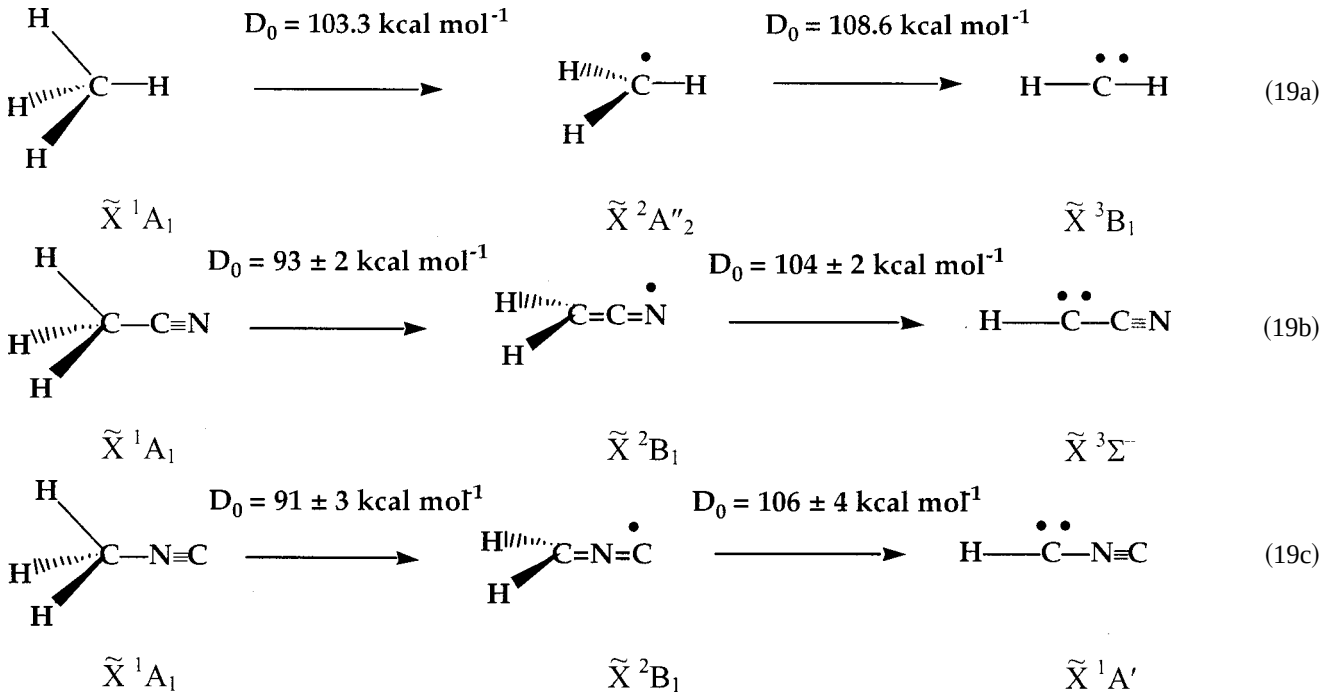

The first bond energy of methane (19a) is 103.3 ± 0.1 kcal mol^{-1} and produces H plus the CH_3 radical; dissociation of CH_3 to produce H and CH_2 requires 108.6 ± 0.5 kcal mol^{-1}. When $CH_3C{\equiv}N$ is considered,[23] the C–H bond energy drops from 103.3 ± 0.1 kcal mol^{-1} to 93 ± 2 kcal mol^{-1} and reflects the allenic nature of the cyanomethyl radical, $CH_2{=}C{=}N\bullet$, $\tilde{X}\,^2B_1$. The 10 kcal mol^{-1} stabilization energy, (103–93), is a typical value for allylic resonance stabilization.[18] Similar arguments[24] apply to the isonitrile, CH_3NC; the C–H bond drops from 103.3 ± 0.1 kcal mol^{-1} to a D_0(H–CH_2NC) of 91 ± 3 kcal mol^{-1}. The second set of C–H bond energies, D_0(H–CHCN) of 104 ± 2 kcal mol^{-1} and D_0(H–CHNC) of 106 ± 4 kcal mol^{-1}, are comparable to that of the CH_3 radical, D_0(H–CH_2) of 108.6 ± 0.5 kcal mol^{-1}. The term values of these carbenes vary wildly from $\Delta E(^1A_1-{}^3B_1)CH_2$; $T_0(CH_2\,\tilde{a}\,^1A_1)=0.392\pm0.002$ eV while $T_0(HCCN\,\tilde{a}\,^1A')=0.515\pm0.016$ eV. However, the ^{3}HCNC and ^{1}HCNC states are inverted in the isocyanocarbene and now $T_0(HCNC\,\tilde{a}\,^3A'')=0.050\pm0.028$ eV.

The $HCCN^-$ photoelectron spectra are compatible with all of the earlier high-resolution microwave[6] and infrared spectra[1–5,7] of ^{3}HCCN, which reveals this species to be a quasilinear molecule.[46,47] The root of the exceptional properties of HCCN $\tilde{X}\,^3\Sigma^-$ is the allylic resonance that is activated by the H–CCN bend, ν_5, as sketched in Eq. (3). This notion would predict that ^{3}HC–C≡CH will also be a quasilinear molecule and will be effectively linear, $\tilde{X}\,^3\Sigma^-$; the singlet will be a bent molecule, HC–C≡CH $\tilde{a}\,^1A'$.

ACKNOWLEDGMENTS

G.B.E. is supported by grants from the Chemical Physics Program, United States Department of Energy (DE-FG02-87ER13695). Some of the electronic structure calculations were supported by a grant from the National Center for Supercomputer Applications (NCSA Grant No. CHE-980028n). W.C.L. is pleased to acknowledge support from the National Science Foundation and the Air Force Office of Scientific Research. C.M.H. is supported by the National Science Foundation (CHE-9733457) and the Ohio Supercomputer Center. G.A.P. is supported by the Department of Energy (DE-FC02-00CH11021) and by Gaussian Inc. The authors are greatly indebted to Michael D. Allen and John M. Brown for several helpful discussions about the spectroscopy of semirigid benders and the FIR-LMR spectra. We have also profited from discussions with Michael C. McCarthy and Jon T. Hougen about the complexities of semirigid benders. Robert F. Curl has been very generous in discussions of his high-resolution IR spectra and in sharing his semirigid bender program together with his HCCN potential that was used to construct Tables I and II. G.B.E. thanks Emily A. Carter for continued discussions about the organic radicals and their valence. We dedicate this paper to our long time friend and NIST colleague, Dr. Kenneth M. Evenson, who passed away on January 29, 2002. Ken was one of the people who made Boulder unique in the world, and all of us will miss him.

APPENDIX: ALTERNATIVE FORMULATIONS OF THE "ACIDITY/EA CYCLE"

The ''acidity/EA cycle'' is a well-known route to the determination of bond energies of polyatomic molecules.[62,63] The purpose of this Appendix is to develop two convenient variations of this cycle.

The enthalpy of deprotonation of a species, RH, is defined[37] as

$$\begin{aligned} &RH \rightarrow R^- + H^+, \\ &\Delta_{acid}H_{298}(RH) = \Delta_f H_{298}(R^-) + \Delta_f H_{298}(H^+) \\ &\qquad - \Delta_f H_{298}(RH). \end{aligned} \tag{A1}$$

The ionization energy, IE(≡ionization potential, IP), is defined by Ervin in his Eq. (8) as

$$\begin{aligned} &H \rightarrow H^+ + e^-, \\ &IE_{298}(H) = \Delta_f H_{298}(e^-) + \Delta_f H_{298}(H^+) - \Delta_f H_{298}(H). \end{aligned} \tag{A2}$$

Likewise the electron affinity, EA, is defined

$$\begin{aligned} &R^- \rightarrow R + e^-, \\ &EA_{298}(R) = \Delta_f H_{298}(e^-) + \Delta_f H_{298}(R) - \Delta_f H_{298}(R^-). \end{aligned} \tag{A3}$$

There is a hidden problem of convention to note in Eqs. (A2) and (A3). We adopt the ''electron convention'' that is defined[37] so that the electron is treated as an element. Consequently the heat of formation is zero at all temperatures; $\Delta_f H_T(e^-) = \Delta_f H_{298}(e^-) \equiv 0$. Since C_p is defined to be $(\partial H/\partial T)_p$, then the ''electron convention'' implies that $C_p(e^-)$ is also zero.

Proton transfer kinetics at 298 K is commonly used to measure the gas-phase acidity, $\Delta_{acid}G_{298}(RH)$, from whence the enthalpy of deprotonation is extracted. We can write an expression that relates the acidity, the bond energy, the IP of H atom, and the electron affinity,

$$\Delta_{acid}H_{298}(RH) = DH_{298}(RH) + IP_{298}(H) - EA_{298}(R). \tag{A4}$$

Kirchhoff's law[37] provides the enthalpy at any temperature *via* the integrated heat capacities; $\Delta_f H_T(R) = \Delta_f H_{0K}(R) + \int dT\, C_p(R)$. Thus we can write the ionization potential as

$$IP_{298}(H) = IP_{0K}(H) + \int dT[C_p(H^+) - C_p(H)], \tag{A5}$$

and the electron affinity similarly

$$EA_{298}(R) = EA_{0K}(R) + \int dT[C_p(R) - C_p(R^-)]. \tag{A6}$$

Consequently the expression for $\Delta_{acid}H_{298}(RH)$ is

$$\begin{aligned} \Delta_{acid}H_{298}(RH) = DH_{298}(RH) &+ \{IP_{0K}(H) \\ &+ \int dT[C_p(H^+) - C_p(H)]\} - \{EA_{0K}(R) \\ &+ \int dT[C_p(R) - C_p(R^-)]\}, \end{aligned} \tag{A7}$$

$IP_{0K}(H)$ has been measured to be 109 678.758(1) cm^{-1} and negative ion photoelectron spectroscopy[60] measures $EA_{0K}(R)$. Thus a working expression can be written

$$\begin{aligned} \Delta_{acid}H_{298}(RH) = DH_{298}(RH) &+ IP_{0K}(H) - EA_{0K}(R) \\ &- \int dT[C_p(R) - C_p(R^-) + C_p(H) \\ &- C_p(H^+)]. \end{aligned} \tag{A8}$$

This is the expression quoted in Ervin *et al.*,[40] Berkowitz *et al.*,[63] and Rienstra-Kiracofe *et al.*[60] If both $\Delta_{acid}H_{298}(RH)$ and EA(R) can be measured and the ion (R^-) and radical (R) are well-behaved molecules, then Eq. (A8) will furnish the bond enthalpy, $DH_{298}(RH)$.

However if one is studying a floppy molecule, such as HCCN, then application of Eq. (A8) is complicated since we must compute $\int dT[C_p(HCCN) - C_p(HCCN^-)]$. The usual route[64] to computing the integrals over heat capacities is to assume that symmetric top rotations and harmonic vibrations approximate the molecule. This is simply not the case for a semirigid bender like HCCN so $\int dT\, C_p(HCCN)$ is a difficult sum.

We can rearrange Eq. (A8), recalling that $DH_{298}(RH) = D_0(RH) + \int dT[C_p(R) + C_p(H) - C_p(RH)]$. Consequently Eq. (A8) becomes

$$\begin{aligned} \Delta_{acid}H_{298}(RH) = D_0(RH) &+ IP_{0K}(H) - EA_{0K}(R) \\ &+ \int dT[C_p(R^-) + C_p(H^+) - C_p(RH)]. \end{aligned} \tag{A9}$$

With this different formulation one uses the experimental values for $\Delta_{acid}H_{298}(RH)$ and EA(R) again, but since Eq. (A9) only uses $\int dT[C_p(R^-) + C_p(H^+) - C_p(RH)]$, we only require that the ion (R^-) and precursor (RH) be well-behaved molecules. If so, then Eq. (A9) will furnish the bond dissociation energy, $D_0(RH)$. Since both $HCCN^-$ and CH_2CN perfectly ordinary species, then $\Delta_{acid}H_{298}(CH_2CN)$, $EA_{0K}(HCCN)$, and $\int dT[C_p(HCCN^-) - C_p(CH_2CN)]$ will produce $D_0(H–CHCN)$.

[1] C. L. Morter, S. K. Farhat, and R. F. Curl, Chem. Phys. Lett. **207**, 153 (1993).
[2] C. E. Miller, W. C. Eckhoff, and R. F. Curl, J. Mol. Struct. **352**, 435 (1995).
[3] F. Sun, A. Kosterev, G. Scott, V. Litosh, and R. F. Curl, J. Chem. Phys. **109**, 8851 (1998).
[4] J. X. Han, P. Y. Hung, J. DeSain, W. E. Jones, and R. F. Curl, J. Mol. Spectrosc. **198**, 421 (1999).
[5] P. Y. Hung, F. Sun, N. T. Hunt, L. A. Burns, and R. F. Curl, J. Chem. Phys. **115**, 9331 (2001).
[6] M. C. McCarthy, C. A. Gottlieb, A. L. Cooksy, and P. Thaddeus, J. Chem. Phys. **103**, 7779 (1995).
[7] M. D. Allen, K. M. Evenson, and J. M. Brown, J. Mol. Spectrosc. **209**, 143 (2001).
[8] W. A. Goddard III, T. H. Dunning, Jr., W. J. Hunt, and P. J. Hay, Acc. Chem. Res. **6**, 368 (1973).
[9] W. A. Goddard III and L. B. Harding, Annu. Rev. Phys. Chem. **29**, 363 (1978).
[10] A. R. W. McKellar, P. R. Bunker, T. J. Sears, K. M. Evenson, R. J. Saykally, and S. R. Langhoff, J. Chem. Phys. **79**, 5251 (1983).
[11] A. R. W. McKellar, P. R. Bunker, T. J. Sears, K. M. Evenson, and S. R. Langhoff, Bull. Soc. Chim. Belg. **92**, 499 (1983).
[12] P. R. Bunker, T. J. Sears, A. R. W. McKellar, K. M. Evenson, and F. J. Lovas, J. Chem. Phys. **79**, 1211 (1983).
[13] G. Herzberg, Proc. R. Soc. London, Ser. A **295**, 106 (1966).
[14] G. V. Hartland, D. Qin, and H.-L. Dai, J. Chem. Phys. **102**, 6641 (1995).
[15] D. G. Leopold, K. K. Murray, A. E. S. Miller, and W. C. Lineberger, J. Chem. Phys. **83**, 4849 (1985).
[16] M. K. Gilles, K. M. Ervin, J. Ho, and W. C. Lineberger, J. Phys. Chem. **96**, 1130 (1992).
[17] E. A. Carter and W. A. Goddard, J. Phys. Chem. **90**, 998 (1986).
[18] G. B. Ellison, G. E. Davico, V. M. Bierbaum, and C. H. DePuy, Int. J. Mass Spectrom. Ion Processes **156**, 109 (1996).
[19] K. M. Ervin, J. Ho, and W. C. Lineberger, J. Chem. Phys. **91**, 5974 (1989).
[20] H. E. K. Matimba, A. M. Crabbendam, S. Ingemann, and N. M. M. Nibbering, Int. J. Mass Spectrom. Ion Processes **114**, 85 (1992).

[21] J. Lee and J. J. Grabowski, Chem. Rev. **92**, 1611 (1992).
[22] F. C. Fehsenfeld, K. M. Evenson, and H. P. Broida, Rev. Sci. Instrum. **36**, 294 (1965).
[23] S. Moran, H. B. Ellis, D. J. Defrees, A. D. McLean, and G. B. Ellison, J. Am. Chem. Soc. **109**, 5996 (1987).
[24] S. Moran, H. B. Ellis, D. J. Defrees, A. D. McLean, S. E. Paulson, and G. B. Ellison, J. Am. Chem. Soc. **109**, 6004 (1987).
[25] D. M. Neumark, K. R. Lykke, T. Andersen, and W. C. Lineberger, Phys. Rev. A **32**, 1890 (1985).
[26] C. E. Moore, *Atomic Energy Levels* (Natl. Bur. Stand., Washington, DC 20402, 1971).
[27] S. T. Graul and R. R. Squires, Mass Spectrom. Rev. **7**, 263 (1988).
[28] B. T. Frink and C. M. Hadad, J. Chem. Soc., Perkin Trans. 2 **11**, 2397 (1999).
[29] M. H. Cohen, C. Barckholtz, B. T. Frink, J. J. Bond, C. M. Geise, J. Hoff, J. Herlinger, T. Hickey, and C. M. Hadad, J. Phys. Chem. A **104**, 11318 (2000).
[30] R. E. Shuster, J. E. Scott, and J. Casanova, Jr., in *Organic Syntheses*, Vol. 5, edited by H. E. Baumgarten (Wiley, New York, 1973).
[31] J. Cooper and R. N. Zare, J. Chem. Phys. **48**, 942 (1968).
[32] J. A. Montgomery, J. W. Ochterski, and G. A. Petersson, J. Chem. Phys. **101**, 5900 (1994).
[33] J. A. Montgomery, M. J. Frisch, J. W. Ochterski, and G. A. Petersson, J. Chem. Phys. **110**, 2822 (1999).
[34] Gaussian 98, Rev. A.7, M. J. Frisch, G. W. Trucks, H. B. Schlegel (Gaussian, Inc., Pittsburgh, 1998).
[35] J. T. Hougen, P. R. Bunker, and J. W. C. Johns, J. Mol. Spectrosc. **34**, 136 (1970).
[36] P. R. Bunker, *Molecular Symmetry and Spectroscopy* (Academic Press, New York, 1979).
[37] K. M. Ervin, Chem. Rev. **101**, 391 (2001).
[38] J. Filley, C. H. Depuy, and V. M. Bierbaum, J. Am. Chem. Soc. **109**, 5992 (1987).
[39] M. Meotner and L. W. Sieck, J. Phys. Chem. **90**, 6687 (1986).
[40] K. M. Ervin, S. Gronert, S. E. Barlow, M. K. Gilles, A. G. Harrison, V. M. Bierbaum, C. H. Depuy, W. C. Lineberger, and G. B. Ellison, J. Am. Chem. Soc. **112**, 5750 (1990).
[41] P. M. Mayer and L. Radom, J. Phys. Chem. A **102**, 4918 (1998).
[42] H. E. K. Matimba, A. M. Crabbendam, S. Ingemann, and N. M. M. Nibbering, Int. J. Mass Spectrom. Ion Processes **114**, 85 (1992).
[43] R. A. Bernheim, R. J. Kempf, P. W. Humer, and P. S. Skell, J. Am. Chem. Soc. **41**, 1156 (1964).
[44] R. A. Bernheim, R. J. Kempf, J. V. Gramas, and P. S. Skell, J. Am. Chem. Soc. **43**, 196 (1965).
[45] A. Dendramis and G. E. Leroi, J. Chem. Phys. **66**, 4334 (1977).
[46] K. S. Kim, H. F. Schaefer III, L. Radom, J. A. Pople, and J. S. Binkley, J. Am. Chem. Soc. **105**, 4148 (1983).
[47] P. A. Malmquist, R. Lindh, B. O. Roos, and S. Ross, Theor. Chim. Acta **73**, 155 (1988).
[48] E. T. Seidl and H. F. Schaefer, J. Chem. Phys. **96**, 4449 (1992).
[49] K. Aoki, S. Ikuta, and O. Nomura, J. Chem. Phys. **99**, 3809 (1993).
[50] M. E. Zandler, J. D. Goddard, and H. F. Schaefer, J. Am. Chem. Soc. **101**, 1072 (1979).
[51] C. B. Kellogg, J. M. Galbraith, J. E. Fowler, and H. F. Schaefer, J. Chem. Phys. **101**, 430 (1994).
[52] B. P. Winnewisser, in *Molecular Spectroscopy: Modern Research, Vol. 3*, edited by K. N. Rao (Academic, Orlando, FL, 1985), p. 321.
[53] P. B. Bernath, *Spectra of Atoms and Molecules* (Oxford University Press, New York, 1995).
[54] J. D. Adamson, J. D. DeSain, R. F. Curl, and G. P. Glass, J. Phys. Chem. A **101**, 864 (1997).
[55] K. Yamada and M. Winnewisser, Z. Naturforsch. A **31**, 131 (1976).
[56] K. Yamada and M. Winnewisser, Z. Naturforsch. A **31**, 139 (1976).
[57] R. F. Curl (unpublished).
[58] G. H. Herzberg, *Molecular Spectra and Molecular Structure: Electronic Spectra and Electronic Structure of Polyatomic Molecules* (D. Van Nostrand, Princeton, New Jersey, 1967).
[59] P. C. Engelking, J. Phys. Chem. **90**, 4544 (1986).
[60] J. C. Rienstra-Kiracofe, G. S. Tschumper, H. F. Schaefer III, S. Nandi, and G. B. Ellison, Chem. Rev. **102**, 231 (2002).
[61] G. Maier, H. P. Reisenauer, and K. Rademacher, Chem.-Eur. J. **4**, 1957 (1998).
[62] C. R. Moylan and J. I. Brauman, Annu. Rev. Phys. Chem. **34**, 187 (1983).
[63] J. Berkowitz, G. B. Ellison, and D. Gutman, J. Phys. Chem. **98**, 2744 (1994).
[64] G. H. Herzberg, *Molecular Spectra and Molecular Structure: Infrared and Raman Spectra of Polyatomic Molecules* (D. Van Nostrand, Princeton, New Jersey, 1945).
[65] J. B. Pedley, R. D. Naylor, and S. P. Kirby, *Thermochemistry of Organic Compounds*, 2nd ed. (Chapman and Hall, New York, 1986).
[66] J. C. Poutsma, S. D. Upshaw, R. R. Squires, and P. G. Wenthold, J. Phys. Chem. A **106**, 1067 (2002).
[67] J. X. Han, P. Y. Hung, J. DeSain, W. E. Jones, and R. F. Curl, J. Mol. Spectrosc. **198**, 5421 (1999).
[68] X. W. An and M. Mansson, J. Chem. Thermodyn. **15**, 287 (1983).
[69] S. G. Lias, J. E. Bartmess, J. F. Liebman, J. L. Holmes, R. D. Levin, and W. G. Mallard, J. Phys. Chem. Ref. Data **17**, 1 (1988).